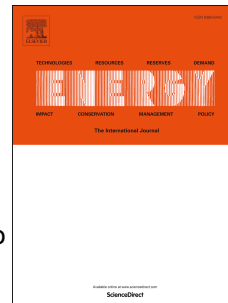


Journal Pre-proof

A potassium responsive numerical path to model catalytic torrefaction kinetics

Edgar A. Silveira, Lucélia A. Macedo, Patrick Rousset, Kevin Candelier, Luiz Gustavo O. Galvão, Bruno S. Chaves, Jean-Michel Commandré



PII: S0360-5442(21)02456-7

DOI: <https://doi.org/10.1016/j.energy.2021.122208>

Reference: EGY 122208

To appear in: *Energy*

Received Date: 30 April 2021

Revised Date: 29 July 2021

Accepted Date: 24 September 2021

Please cite this article as: Silveira EA, Macedo LA, Rousset P, Candelier K, Galvão LGO, Chaves BS, Commandré J-M, A potassium responsive numerical path to model catalytic torrefaction kinetics, *Energy*, <https://doi.org/10.1016/j.energy.2021.122208>.

This is a PDF file of an article that has undergone enhancements after acceptance, such as the addition of a cover page and metadata, and formatting for readability, but it is not yet the definitive version of record. This version will undergo additional copyediting, typesetting and review before it is published in its final form, but we are providing this version to give early visibility of the article. Please note that, during the production process, errors may be discovered which could affect the content, and all legal disclaimers that apply to the journal pertain.

© 2021 Elsevier Ltd. All rights reserved.

Credit Author Statement (Author - Contribution)

Edgar A. Silveira: Conceptualization, Investigation, Formal analysis, Methodology, Writing - original draft.

Lucélia A. Macedo: Data curation, Investigation, Methodology, Formal analysis, Writing - review & editing.

Patrick Rousset: Writing - review & editing, Project administration, Supervision.

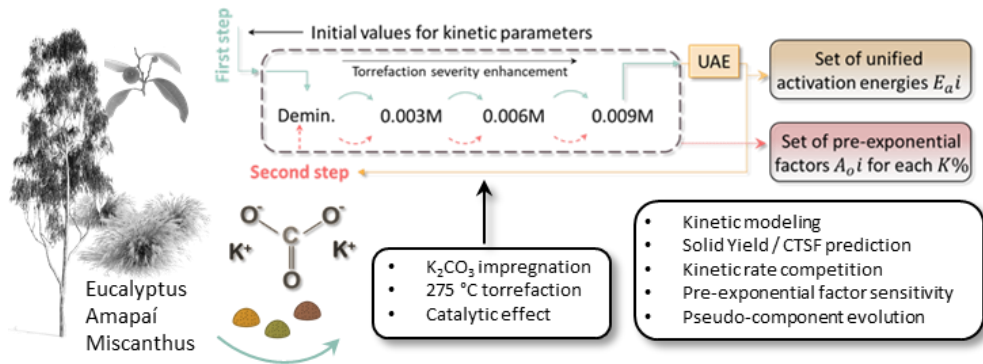
Kevin Candelier: Validation, Writing - review & editing.

Jean-Michel Commandré: Writing - review & editing, Project administration.

Luiz Gustavo O. Galvão: Writing - review & editing.

Bruno S. Chaves: Writing - review & editing.

Graphic abstract



1 A potassium responsive numerical path to model catalytic torrefaction kinetics

2 Edgar A. Silveira ^{a*}, Lucélia A. Macedo ^b, Patrick Rousset ^{c,d}, Kevin Candelier ^{c,d}, Luiz
3 Gustavo O. Galvão ^b, Bruno S. Chaves ^b, Jean-Michel Commandré ^{c,d}.

4
5 a. Mechanical Engineering Department, University of Brasília, Brasília, DF 70910-900, Brazil.

6 b. Forest Products Laboratory, Brazilian Forest Service, 70818900, Brasília, Brazil.

7 c. CIRAD, UPR BioWooEB, F-34398 Montpellier, France.

8 d. BioWooEB, Univ. Montpellier, CIRAD, Montpellier, France.

9 * Corresponding author e-mail: edgar.silveira@unb.br

10 Abstract

11 To assess the potassium catalytic influence on the kinetic behavior of non-oxidative
12 biomass torrefaction, two woody biomass samples (*Amapaí* and *Eucalyptus*), as well as
13 *Miscanthus* samples impregnated with three different K₂CO₃ concentrations (0.003M,
14 0.006M, and 0.009M) were comprehensively studied. The solid thermal degradation
15 kinetics were analyzed through thermogravimetric analysis in usual torrefaction
16 conditions (275 °C during 68min and 10 °C.min⁻¹ heating rate) and an original
17 Potassium Responsive Numerical Path (PRNP). Therefore, a two-step reaction model
18 with unified activation energies was integrated within a numerical method that considers
19 the torrefaction severity influence for each potassium-loading content in all three
20 biomasses. The proposed PRNP enables an accurate solid yield prediction ($R^2 > 0.9995$).
21 A strong (R^2 between 0.91–0.99) and a significant ($p \leq 0.0463$) linear correlation was
22 highlighted between the potassium content in biomass, the increasing reaction rates, and
23 pre-exponential factors. The solid and volatile product distribution depicted faster and
24 marked degradation for solid pseudo-components and anticipated a higher volatile
25 release. The catalytic torrefaction severity factor determination enabled correlating
26 treatment severity and kinetic rates showing better correlations than K% for wood
27 biomass. The accurate results are conducive to developing numerical models that are
28 essential for assessing solid fuel upgrading under catalytic effect in torrefaction plants.

29 **Keywords:** Torrefaction, potassium impregnation, catalytic effect, kinetic model, unified

30 activation energy, catalytic torrefaction severity factor.

31

| Index summary | | | |
|------------------------------------|---|------------------------|-------------------------------------|
| <i>A</i> | Feedstock | <i>M</i> | Molar concentration |
| <i>A_{0i}</i> | Pre-exponential factor | PRNP | Potassium responsive numerical path |
| <i>B</i> | Intermediate solid | <i>R</i> | Gas constant |
| <i>C</i> | Solid residue | <i>R_{CC}</i> | Linear correlation coefficient |
| <i>CO</i> | Carbon monoxide | <i>R²</i> | Coefficient of determination |
| <i>CO₂</i> | Carbon dioxide | <i>T</i> | Temperature |
| <i>CTSF</i> | Catalytic torrefaction severity factor | <i>t</i> | Time (min) |
| DTG | Derivative of thermogravimetric | <i>T_H</i> | Reaction temperature |
| <i>E_{ai}</i> | Activation energy (J.mol ⁻¹) | TGA | Thermogravimetric analysis |
| FTIR | Fourier-transform Infrared spectroscopy | UAE | Unified Activation Energy |
| ICP-AES | Inductively Coupled Plasma-Atomic Emission Spectrometry | <i>V₁</i> | First step volatile product |
| <i>K₂CO₃</i> | Potassium carbonate | <i>V₂</i> | Second step volatile product |
| <i>K%</i> | Potassium content | <i>α_{cat}</i> | Catalytic alpha |
| <i>k_i</i> | Reaction rate | WL | Weight loss |
| | | <i>Y</i> | Yield |

32

33

34

35

36

37

38

39

40

41

42

43

44 1. Introduction

45 Given the growing threat of climate change and the depletion of fossil-fuel sources,
46 it is imperative to diversify the energy profile, whereby biomass represents one of the
47 most appealing options as it is carbon-neutral [1]. Biomass as a renewable, non-fossil,
48 and CO₂ neutral solid fuel has several inherent challenges: high moisture and oxygen
49 content, low energy density, its hydrophilic nature, and its highly variable composition
50 and properties [2]. Biomass thermochemical conversion is a feasible pathway to
51 overcome these issues [3]. Furthermore, the use of biomass can be enhanced through
52 thermochemical processes, such as torrefaction, pyrolysis, and gasification, thus
53 reducing unwanted by-products by process parameter optimization [2–5].

54 Torrefaction is a thermal treatment usually conducted in non-oxidative or partially
55 oxidative conditions where the biomass is mildly pyrolyzed at 200–300 °C seeking an
56 upgraded solid fuel [6–8]. The literature reports torrefaction studies exploring the effects
57 on the physicochemical properties of biomass [9,10], its solid and energy yields, and the
58 increase in energy densification [11–14]. There is also evidence that the thermal
59 treatment enhances the grindability, hydrophobicity, decay resistance, and storage
60 performance of biomass [15–18]. As a consequence, the use of torrefied biomass may
61 tackle agricultural purposes, such as soil amendment [19], and industrial applications,
62 such as ironmaking, pyrolysis, liquefaction, gasification, combustion, ignitability,
63 pollutant adsorption and the mitigation of environmental hazards [8,20–23].

64 Raw biomass naturally contains distinct amounts of alkali and alkaline earth metals
65 depending on the species, the fraction of the biomass, and the soil [24]. Potassium is a
66 well-known alkali catalyst in the thermal reactions of biomass [25]. Previous studies
67 applied analytical techniques, such as thermogravimetric analyzer (TGA) and its
68 derivative (DTG), X-ray diffraction analysis, pyrolysis–gas chromatography–mass

69 spectrometry (Py-GC/MS), and Fourier-transform Infrared spectroscopy (FTIR) to
70 extensively analyze the catalytic effects of potassium on biomass thermochemical
71 conversion processes [24,26–38].

72 Past studies suggested that potassium impregnation can intensify biomass thermal
73 degradation processes by catalytically influencing the decomposition and char
74 conversion mechanisms [24,26–28,31–38]. In addition, the catalytic effect of biomass
75 with higher potassium contents could allow shorter residence times in future torrefaction
76 plants as well as lower temperatures to obtain the desired solid yield [24,26,32,34].

77 The thermal-degradation kinetic modeling has been extensively assessed to
78 characterize the behavior in the thermal decomposition of woody biomass, describing the
79 reaction pathway during torrefaction [25,39–44]. Regarding numerical modeling of
80 lignocellulosic pyrolysis kinetic, generally, non-isothermal and isothermal kinetics are
81 two basic modes. Several approaches to iso-thermal kinetics, such as one [45,46], two
82 [25,42,47–53], multi-step [54–58], and multi-component [59] models have been
83 developed. The literature also presents studies on the potassium content effect on
84 Pyrolysis kinetics [58,60,61].

85 Guo et al. (2016) investigated the potassium impregnation effect (0.1, 0.3, and 0.5
86 mol.kg⁻¹) on the pyrolysis kinetics of pinewood through TGA and fixed bed reactor
87 techniques and the Flynn-Wall-Ozawa numerical method [60]. The results revealed that
88 biomass potassium impregnation leads to higher reactive activity that promotes biomass
89 decomposition [60]. The activation energy was evaluated for different conversion rates
90 α and, concerning the main reaction stage ($0.3 < \alpha < 0.7$), slight variations were
91 evidenced for the activation energy. When α varied between 0.2 and 0.8, the averaged
92 activation energy was similar for different $K\%$ loading with 157.4, 160.3, and 157
93 kJ.mol⁻¹ for 0.1, 0.3, and 0.5 mol.kg⁻¹, respectively [60].

94 Lin et al. (2021) applied the rubberwood pyrolysis experimental results from [34] to
95 explore the pyrolysis kinetics by an independent parallel reaction model describing the
96 catalytic effect on the four pseudo-component [61]. Pyrolysis kinetics results showed
97 that the highest K_2CO_3 concentration (0.012M) reduced the activation energy of
98 cellulose, from 223.86 to 204.14 $\text{kJ}\cdot\text{mol}^{-1}$, whereas there was no noticeable effect on the
99 activation energies of hemicelluloses and lignin [61].

100 Concerning biomass torrefaction kinetics, Di Blasi and Lanzetta (1997) [49]
101 proposed a well-known reaction model to determine the isothermal kinetics. The two-
102 step model was widely explored to describe the behavior of various types of
103 lignocellulosic biomasses, such as willow [50,62,63], wheat straw [47], beech, pine,
104 wheat [48], spruce, and birch [51] submitted to different torrefaction conditions. In
105 addition, a thermal sensitivity three-stage approach based on [49] was adopted to
106 describe the behavior of poplar, fir [25,42,43], and *Eucalyptus grandis* degradation
107 [52,53,64,65], showing prediction accuracy for a wide range of torrefaction parameters.

108 Shoulaifar et al. (2016) modeled the thermal degradation reactions of spruce with
109 distinct $K\%$ content by using a two-step reaction model based on four kinetic rate
110 constants during torrefaction [26]. The study evidenced that the activation energies of
111 each reaction step are quite similar despite the different K contents, whereas the pre-
112 exponential factors do vary with $K\%$ [26]. The results also showed that the mass loss of
113 spruce biomass impregnated with different levels of $K(\%)$ could be modeled using the
114 same activation energies but distinct pre-exponential factors for the kinetic rate
115 constants; the so-called Unified Activation Energy (UAE) [26].

116 Considering the two-step reaction mechanism, eight parameters (four activation
117 energies and four pre-exponential factors) must be considered during each biomass and
118 potassium impregnation modeling routine. Applying the UAE, Shoulaifar et al. (2016)

119 showed that a good prediction was obtained with a minor number of input parameters,
120 simplifying the numerical routine for catalytic torrefaction. The UAE was performed by
121 averaging the obtained activation energy values for five torrefaction temperatures (240,
122 250, 260, 270, and 280 °C) considering spruce wood samples doped with different levels
123 of K [26]. The model was validated against experimental TG curves of straw, spruce
124 wood and bark, aspen, and miscanthus [26]. The results showed a good agreement
125 between the model and experiments for analyzed biomasses, except for spruce bark [26].

126 Although notable results were reported on the impact of potassium impregnation on
127 thermal degradation behavior for different thermochemical conversion routes (mainly
128 based on gasification and fast pyrolysis processes), it is observed that few studies have
129 been performed for torrefaction treatment. Moreover, the literature review found that
130 only some studies have been performed for the kinetic modeling of biomass torrefaction
131 under catalytic effect. Thus, knowledge in recognizing the kinetic mechanisms of
132 catalytic torrefaction and accurately predicting thermal degradation behavior, and
133 torrefied product properties of biomass impregnation by potassium, still remains limited.

134 Therefore, to extend the knowledge on kinetic modeling prediction for catalytic
135 torrefaction, this study investigates the thermal degradation kinetics in three different
136 types of biomasses, proposing a novel potassium responsive numerical path (PRNP) in
137 combination with the UAE. In addition, it shows the linear behavior of the predicted
138 kinetic rates and pre-exponential factors with increasing potassium content with the
139 application of two performance indicators; the catalytic torrefaction severity factor
140 (CTSF) and the K%.

141 Hence, the present work allows for characterizing the catalytic effect of three
142 concentrations of potassium carbonate (K_2CO_3) impregnation on the non-oxidative
143 torrefaction kinetics. The results provide the kinetic rates, solid yield prediction, the

144 linear correlation statistics between the pre-exponential factors A_0i and $K\%$ content, the
145 CTSF [30], and the solid and volatile product distribution. The results achieved are also
146 valuable for assessing the impact of catalytic torrefaction on solid fuel upgrading and
147 the produced volatiles. Therefore, providing essential insights on modeling optimization
148 in the energy field for circular bioeconomy.

149 2. Material and Methods

150 2.1 Biomass feedstock and preparation

151 This work was conducted on three biomass materials: *Amapaí* (*Brosimum potabile*
152 Ducke) and a 7.5-year-old *Eucalyptus* hybrid clone (*E. urophylla* and *E. camaldulensis*)
153 as woody species, as well as *Miscanthus* pellets as herbaceous species. The *Eucalyptus*
154 material was selected because it is the most widely planted wood species in Brazil, with
155 planted forest area of five million hectares [66,67]. The chosen *Eucalyptus* clone is
156 prevalent and planted mainly for charcoal production. *Miscanthus* was selected because
157 it is one of the most promising fast-growing second-generation types of biomass for
158 energy purposes [68]. The third species, *Amapaí*, can be developed in Brazilian forest
159 concession projects that seek to replace the predatory exploitation model with a
160 sustainable management model [28]. In addition, the physical and chemical
161 characterization of the *Amapaí* species is still little explored in the literature.

162 Table 1 displays the results from the inorganic element analysis performed by the
163 Inductively Coupled Plasma-Atomic Emission Spectrometry (ICP-AES), as well as from
164 the ultimate and proximate analyses of the raw biomass samples obtained in our previous
165 work [28,32], which also include the procedure guidelines.

166 Table 1

167 2.2 Physical-chemical sample preparation

168 The raw materials were grounded and sieved by an 18-mesh screen (<1mm). After
169 that, all samples were oven-dried (105 °C for 24h), demineralized, and impregnated with
170 K₂CO₃ aqueous solutions of three different concentrations (0.003M, 0.006M and
171 0.009M). The K₂CO₃ solution concentrations were defined according to the range in
172 which the potassium loading effect in the torrefaction degradation kinetics is more
173 pronounced [24]. The potassium content within biomass samples varied from 0% to
174 0.53%, corresponding to the demineralized and different K₂CO₃ concentrations. Biomass
175 samples were categorized corresponding to the K₂CO₃ concentration of the impregnation
176 solution in which they were immersed [32]. The description on demineralization and
177 impregnation processes is available in a previous study [32]. All samples used in this
178 study are presented in Table 2, according to their K content (in %, dry basis).

179 **Table 2**

180 2.3 Thermo-gravimetric analyses (TGA)

181 The thermogravimetric analysis (TGA) results of demineralized and potassium
182 impregnated herbaceous (*Miscanthus*) and hardwoods (*Amapaí* and *Eucalyptus*) from
183 [32] provided the material for this work. The thermo-gravimetric analyzer described in
184 [32,69–71] was used to record (10⁻⁴ g precision balance) weight loss of samples
185 throughout the torrefaction treatment under non-oxidative conditions (0.5 L.min⁻¹ N₂
186 flow) [32]. In order to avoid diffusion limitations within the alumina crucible, about 100
187 ± 15 mg of samples were used for each experiment. All experiments were duplicated for
188 each demineralized (control) and potassium-loaded biomass sample. Samples were first
189 heated (10 °C.min⁻¹) from 25 to 105 °C and isothermally kept for 30 min to ensure dry
190 conditions before torrefaction [32]. After that, a 10 °C.min⁻¹ heating rate was
191 implemented until reaching the treatment temperature of 275 °C [32]. Isothermal
192 torrefaction step was then carried out for 50 min.

193 The TGA was evaluated overtime t for the 275 °C treatment temperatures and
 194 different potassium impregnation. The calculated solid yield $Y_{exp}^{275^{\circ}C}_{K\%}(t)$ for the
 195 constantly weighted wood sample was determined by the ratio of dried weight before
 196 torrefaction w_0 and the weight during torrefaction $w_i(t)$, according to Equation (1)
 197 [42,72].

$$198 \quad Y_{exp}^{275^{\circ}C}_{K\%}(t) = \frac{w_i(t)}{w_0} \times 100 \quad (1)$$

199 2.4 Catalytic torrefaction severity factor (CTSF)

200 The torrefaction literature presents the efficiency of biomass torrefaction processes by
 201 proposing severity indexes to discuss the variability of thermally modified biomass
 202 properties [73,74]. In this work, the parameter of the catalytic torrefaction severity index
 203 [30,75] is also introduced to assess the catalytic thermo-degradation phenomena during
 204 the torrefaction process. The CTSF is an operating condition-based index that aggregates
 205 the catalytic influence of $K\%$ and biomass sensitivity on the treatment severity. The
 206 detailed procedure for CTSF and catalytic alpha α_{cat} determination is exposed in
 207 previous work [30]. The CTSF is defined by the following Equations (2) and (3):

$$208 \quad CTSF_{K\%}(t) = \log \left[t^{\alpha_{cat}} \times \exp \left(\frac{T_H}{14.75} \right) \right] \quad (2)$$

$$209 \quad \alpha_{cat} = \alpha + K(\%) \quad (3)$$

210 where $K\%$ is the potassium impregnation content (demi, 0.003M, 0.006M and 0.009M),
 211 t is the treatment time (min), T_H is the reaction temperature (275 °C for this study), and
 212 α_{cat} is the optimum value achieved when analyzing the coefficient of determination R^2
 213 dependence when altering the α_{cat} time exponent [30,76]. The α_{cat} time exponential
 214 originates from the α value modification by adding the potassium concentration to the
 215 original TSF α value [74]. This modification enables maintaining the same linear

216 behavior introduced by the $K\%$ impregnation and accounts for the catalytic behavior and
 217 the other severity parameters (temperature, time, and feedstock sensitivity) [30].

218 The CTSF was selected as a performance indicator because it aggregates the key
 219 performance indicators (temperature, time, biomass nature, and catalysis) regarding
 220 torrefaction severity and is an index that only depends on the process parameters
 221 (established before experiments), enabling practical and accurate torrefaction
 222 performance prediction under catalytic effect [30].

223 2.5 Kinetic numerical modeling

224 The numerical modeling was established based on the consecutive two-step reaction
 225 proposed by [49] and well-validated in previous work [48,50,51,53,77]. The two-step
 226 model was selected due to its precision and simplicity in predicting biomass torrefaction
 227 in a wide range of parameters [25,26,42,53]. The past study [42,53] employed the two-
 228 step model within a three-stage approach, considering the sensitivity of torrefaction
 229 severity within the model's convergence, optimizing simulation quality with reasonable
 230 computation time. The two-step consecutive reactions [49] were considered as Equations
 231 (4) and (5).



234 where A is the feedstock (raw material), B is the intermediate solid, and C is the solid
 235 residue [49]. Experimentally, a decrease in weight loss is numerically established through
 236 the volatile V_1 released during the first step and V_2 during the second step [42]. The solid
 237 pseudo-component composition (A , B , and C) must correspond to 100% of the predicted

238 solid yield at any time [53]. The first step accounts for the hemicelluloses degradation
 239 and the removal of extractives [49]. In parallel, the hemicelluloses, cellulose, and part of
 240 lignin degradation are considered by the second step [56].

241 The calculation of the pseudo-components $Y_{n,cal}^{(275^\circ C)}_{K\%}$ with $n = A, B, C, V_1, V_2$ for each
 242 potassium concentration $K\%$ was conducted with Equations (6–10).

$$243 \quad Y_{A,cal}^{(275^\circ C)}_{K\%}(t) = \frac{dm_A(t)}{dt} = -(k_1 + k_{V_1}) \times m_A(t) \quad (6)$$

$$244 \quad Y_{B,cal}^{(275^\circ C)}_{K\%}(t) = \frac{dm_B(t)}{dt} = k_1 \times m_A(t) - (k_2 + k_{V_2}) \times m_B(t) \quad (7)$$

$$245 \quad Y_{C,cal}^{(275^\circ C)}_{K\%}(t) = \frac{dm_C(t)}{dt} = k_2 \times m_B(t) \quad (8)$$

$$246 \quad Y_{V_1,cal}^{(275^\circ C)}_{K\%}(t) = \frac{dm_{V_1}(t)}{dt} = k_{V_1} \times m_A(t) \quad (9)$$

$$247 \quad Y_{V_2,cal}^{(275^\circ C)}_{K\%}(t) = \frac{dm_{V_2}(t)}{dt} = k_{V_2} \times m_B(t) \quad (10)$$

248 The kinetic rate constants k_i (min^{-1} , $i = 1, 2, V_1, V_2$) are defined by the Arrhenius law
 249 as a function of the pre-exponential factor A_0i (min^{-1}), the activation energy E_{a_i}
 250 ($\text{kJ}\cdot\text{mol}^{-1}$), and the temperature $T(\text{K})$, as displayed in Equation (11). The rates were
 251 determined by fitting experimentally measured TG profiles $Y_{exp}^{275^\circ C}_{K\%}(t)$ to predicted
 252 curves $Y_{solid,cal}^{275^\circ C}_{K\%}(t)$.

$$253 \quad k_i = A_0i \times e^{-E_{a_i}/RT} \quad (11)$$

254 where R is the gas constant ($\text{J}\cdot\text{mol}^{-1}\cdot\text{K}^{-1}$). The numerical predicted solid $Y_{solid,cal}^{275^\circ C}_{K\%}(t)$
 255 and volatile $Y_{volatile,cal}^{275^\circ C}_{K\%}(t)$ yields were established by the sum of the calculated
 256 pseudo-components for each $K\%$ with Equations (12) and (13).

$$257 \quad Y_{solid,cal}^{(275^\circ C)}_{K\%}(t) = Y_{A,cal}^{(275^\circ C)}_{K\%}(t) + Y_{B,cal}^{(275^\circ C)}_{K\%}(t) + Y_{C,cal}^{(275^\circ C)}_{K\%}(t) \quad (12)$$

$$258 \quad Y_{volatile,cal_{K\%}}^{(275^{\circ}C)}(t) = Y_{V_1,cal_{K\%}}^{(275^{\circ}C)}(t) + Y_{V_2,cal_{K\%}}^{(275^{\circ}C)}(t) \quad (13)$$

259 The numerical modeling using Matlab® was performed to determine all kinetic
260 parameters, solid and volatile product distributions and the predicted yields [53].

261 2.6 Potassium responsive numerical path (PRNP)

262 Previous work analyzed the kinetic behavior by evaluating the activation energies for
263 different potassium concentrations and specific pyrolysis conditions [58,60,61].
264 Regarding the temperature range of 200–300 °C (characteristic of torrefaction) and the
265 potassium concentration limits of the present study, the reported results in [58,60,61]
266 showed no noticeable (or even slight) variations in the obtained activation energies.

267 Based on these findings, this work proposes an original potassium responsive
268 numerical path (PRNP) to characterize the kinetic behavior of three biomasses
269 impregnated with distinct potassium content. The proposed PRNP numerical path is
270 structured based on two methods. The first is the three-stage approach, where the biomass
271 thermal degradation sensitivity (due to torrefaction temperature) is considered for each
272 step [42]. The second is the UAE, where the model is established using the same
273 activation energies but distinct pre-exponential factors for the kinetic rate constants [26].
274 Thus, the reported catalytic effect promoted by K_2CO_3 [32] (faster degradations and
275 higher weight loss) is considered through the PRNP by pondering the degradation
276 sensitivity promoted by each degree of potassium content in the biomass. As a
277 consequence, the PRNP enables an even more accurate prediction using a minor number
278 of kinetic parameters.

279 The UAE was conducted considering unified activation energies for the three
280 biomasses despite the distinct pre-exponential factors for each degree of potassium
281 impregnation. The method is schematically illustrated in Figure 1.

282

Figure 1

283 Firstly, the kinetic parameters were separately determined for each of the four
284 potassium conditions in the first step. An initial parameter for the reaction rates is required
285 for conducting the numerical prediction when applying the PRNP. Therefore, the reaction
286 rates of *Eucalyptus grandis* torrefaction at 270 °C from a previous study were applied due
287 to the similar biomass and treatment temperature [53,64], enabling the determination of
288 kinetic rates of demineralized *Eucalyptus* hybrid clone with the numerical routine
289 exposed in Section 2.5.

290 The resulting kinetic rates of demineralized *Eucalyptus* hybrid clones were used as
291 initial conditions for 0.003M potassium content, the 0.003M results for 0.006M, and the
292 last for the 0.009M. This first routine describes the first step of the PRNP (green arrows
293 in Figure 1). The kinetic rates obtained for demineralized *Eucalyptus* hybrid clones were
294 used as initial parameters for demineralized *Amapaí* and *Miscanthus*. The first step was
295 conducted for each biomass species separately. The attained results for each of the three
296 biomasses showed similar activation energies of each reaction step, in agreement with
297 [26].

298 Before the second step, the UAE was applied by averaging the obtained activation
299 energies [26] in the PRNP first step, defining one set of unified activation energies for the
300 three biomasses. Finally, during the second step (red dashed arrows in Figure 1), the
301 numerical kinetic modeling routine (Section 2.5) was again performed for each K%
302 content and biomass species with the calculated set of unified activation energies,
303 obtaining the final set of pre-exponential factors for each condition and biomass.

304 3. Results and discussions

305 The obtained activation energies, pre-exponential parameters, as well as the R^2
 306 between experimental and predicted curves from PRNP, are shown in Table 3. Figure
 307 2(a), (b), and (c) display experimental [32] and predicted values by the PRNP of the solid
 308 yield evolution during torrefaction for *Amapaí*, *Eucalyptus*, and *Miscanthus*, respectively.
 309 The sample weight was normalized (considered as 100%) at treatment temperature of
 310 170 °C (the temperature that characterizes the start of thermal degradation) since no
 311 considerable degradation occurred before this temperature was reached [25,42].
 312 Therefore, in Figure 2, $t = 0$ corresponds to the treatment time at which the temperature
 313 is 170 °C. As observed, the UAE performed within the PRNP obtained a highly accurate
 314 fit with correlation coefficients of $R^2 \geq 0.9995$ for all potassium impregnation levels and
 315 all three biomasses.

316 Table 3

317 The achieved unified activation energies, expressed in $\text{J}\cdot\text{mol}^{-1}$, for the first and second
 318 step, were $E_{a1} = 82307.1$, $E_{aV1} = 149275.2$, $E_{a2} = 35491.1$, and $E_{aV2} = 124583.9$,
 319 which is in line with the range obtained for *Eucalyptus grandis* in [53] and reported in the
 320 literature [50,78]. The originally proposed two-step model by [49] and [53] reports higher
 321 values for the first reaction step's activation energy when compared to the second step,
 322 which is in agreement with our results and indicates that the second step has a lower
 323 temperature dependency than the first step. When comparing volatile and solid activation
 324 energies, those for the volatile release (E_{aV1} and E_{aV2}) are higher than those for the solid
 325 conversion (E_{a1} and E_{a2}), corroborating with [25,49,52,53].

326 Figure 2

327 3.1 Catalytic effect on the reaction rate competition

328 For a better interpretation of the competition rate between the occurring reactions, the
329 calculated reaction rate constants (Table 3) are graphically displayed against the $K\%$ in
330 Figure 2(d), (e), and (f) for *Amapaí*, *Eucalyptus*, and *Miscanthus*, respectively.

331 For the three species, an increasing linear correlation between reaction rates and
332 potassium content was obtained. Shoulaifar et al. (2016) reported that the pre-exponential
333 factors of k_1 , k_{V_1} , and k_{V_2} have increasing linear correlations with the growing potassium
334 content but decreased k_2 . Unlike [26], the results show an increased correlation between
335 potassium content and k_2 , accelerating reactions when the $K\%$ increases. These results
336 are in line with the experimental results that presented lower solid yields and
337 intensification of non-condensable gas and water release for higher potassium contents
338 [32,36,79].

339 The first step reaction rates k_1 and k_{V_1} (mainly hemicellulose decomposition) become
340 faster with higher $K\%$, which is in line with [24,26]. Regarding the literature on
341 torrefaction treatment, the evidenced ranking of reactions is $k_1 > k_{V_1}$ during the first step
342 [25,42,49–51], corroborating with the results. The first step reaction rate behavior is in
343 line with the pyrolysis kinetics of rubberwood [61], which showed a slight increase of
344 reaction rates with the potassium concentration (0.004M, 0.008M, and 0.012M) during
345 thermal degradation of the hemicelluloses. The obtained reaction rates in the first step
346 also corroborate with the pyrolysis experiments from [80], which reported a slight
347 increase of the hemicelluloses reaction temperature as the K_2CO_3 concentration
348 increased.

349 The second step reaction was ascribed mainly to cellulose, remaining hemicelluloses
350 and part of lignin degradation [41]. The previous studies [25,42,43,53] reported that k_2 is
351 faster than k_{V_2} during the second step reaction for torrefaction treatment. For higher

352 temperatures (or torrefaction severity), k_{V_2} becomes as important as k_2 [52,53]. In Figure
353 2(d), (e), and (f), the catalytic effect on the second step is observed with faster k_{V_2} for
354 higher potassium content in biomass, with $k_{V_2} > k_2$ from 0.23 and 0.14 K% for *Amapaí*
355 and *Miscanthus*, respectively.

356 Regarding *Eucalyptus* experiments, the k_{V_2} was faster for increasing catalytic content
357 and, therefore, the torrefaction severity. Analyzing the TGA curves for *Eucalyptus* and
358 separated cellulose component, the previous work [32] evidenced that the catalytic effect
359 (anticipated degradation) increased for biomass impregnated by potassium, indicating
360 that this behavior might be attributed to changes in cellulose decomposition induced by
361 K_2CO_3 . The results are in line with [53], which presented faster k_{V_2} with increasing
362 torrefaction severity (temperature) for *Eucalyptus*. In addition, Chen et al. (2021)
363 analyzed the two-step reaction model to predict the isothermal torrefaction kinetics of
364 cellulose when applying TG-FTIR. Their results showed that, for higher severities of
365 torrefaction, the related V_2 formation associated with cellulose degradation is higher,
366 corroborating with the faster k_{V_2} obtained under the potassium catalytic conditions [81].
367 Therefore, such a result can be related to *Eucalyptus* wood composition (Table 1) that
368 presents higher cellulose content compared to the other two biomasses.

369 Given the catalytic effect, with increased potassium content, a more important second
370 step is thus obtained (Figure 2). This behavior is consistent with the experimental results
371 [24,32], which showed an increased weight loss and therefore a greater volatile release
372 and faster conversion rates, illustrated by the shift in the DTG peak for cellulose from 44
373 to 24 min (from 275 to 262 °C). Studies [36,79] also indicated higher CO, CO₂ and water
374 release for experiments above 250 °C. The reaction rate behavior obtained with the PRNP
375 in the second step is in line with the reported literature.

376 Comparing the reaction rates for impregnated samples (0.003, 0.006, and 0.009M)
377 between species, the first step showed *Amapaí* > *Eucalyptus* > *Miscanthus* for k_1 and
378 *Eucalyptus* > *Amapaí* > *Miscanthus* for k_{V_1} . Considering the second step, solid and
379 volatile reaction rates (k_2 and k_{V_2}) followed the same order for increasing potassium
380 content retained in the biomass samples [24,32], showing that *Amapaí* > *Miscanthus* >
381 *Eucalyptus*.

382 3.2 Reaction rates and pre-exponential factor statistics

383 Table 4 shows the correlation statistics for the reaction rates against the $K\%$ content.
384 A strong linear correlation (R^2 varying between 0.91 and 0.99) and statistical significance
385 (p -values < 0.0448) was emphasized for all the cases. The results show, for instance, that
386 $k_i = A \times K(\%) + B$ can correctly estimate the two-step reaction rates with $K\%$ content
387 varying from 0–0.39, 0–0.53, and 0–0.40% for *Amapaí*, *Eucalyptus*, and *Miscanthus*,
388 respectively.

389 **Table 4**

390 The obtained values for the pre-exponential factors (Table 3) are illustrated in Figures
391 3 and 4. Based on the molecule collision theory, the pre-exponential factor is an important
392 term correlated to the molecules' rate of collision and their average velocity [61]. Hence,
393 for a specific reaction, the higher the pre-exponential factor, the more frequent collisions
394 would be observed for that reaction, and the reaction successfully occurs more often [61].
395 Higher pre-exponential factors were evidenced with increasing potassium content for
396 both reaction steps and all biomasses.

397 **Figure 3**

398 **Figure 4**

399 The obtained linear correlation statistics for the pre-exponential factor's linear

400 dependency of the potassium content are given in Table 5. Regarding Table 5, the PRNP
 401 resulted in an accurate linear correlation ($0.90 < R^2 < 0.99$) with significance ($p \leq 0.0463$)
 402 through increasing exponential factors with potassium content for the three biomasses, in
 403 agreement with [26]. Chemically, the high pre-exponential factor of a reaction may
 404 illustrate that the required reaction time is shorter for a given temperature or that the
 405 reaction occurs within a narrow temperature range [61]. The torrefaction experimental
 406 results [24,32] evidenced increased weight loss and faster conversions (anticipated DTG
 407 peaks) with higher K content, corroborating with the higher pre-exponential factor
 408 behavior. The correlations in Table 5 presented statistical significance for all the cases
 409 where the p -value was lower than 0.0463 and R^2 between 0.91 and 0.99, considering the
 410 three potassium contents and all three biomasses.

411 **Table 5**

412

413 3.3 Catalytic torrefaction severity factor

414 The CTSF was calculated to provide a useful performance indicator to be correlated
 415 with the obtained kinetic parameters. The obtained results for *Amapaí* and *Eucalyptus*
 416 CTSF from [30] were used in this analysis. *Miscanthus* CTSF was defined with the same
 417 modeling procedures. The obtained values for the α_{cat} and CTSF for the torrefied
 418 products are given in Table 6. For instance, woody biomasses had similar α_{cat} , with 2.0
 419 for *Amapaí* and 1.9 for *Eucalyptus*, while α_{cat} of *Miscanthus* is 2.8, which is distinctly
 420 higher than those of the two previous hardwood species.

421

Table 6

422 The α_{cat} accounts for inherent biomass sensitivity and its potassium content [30,74].
 423 *Miscanthus* presented higher α_{cat} , which is in line with the experimental results for raw

424 biomass that shows higher weight loss with higher torrefaction severity for *Miscanthus*
 425 when compared to both woody biomasses [24,32].

426 Figure 5(a), (b), and (c) displays the CTSF three-dimension surfaces of *Amapaí*,
 427 *Eucalyptus*, and *Miscanthus*, respectively. The CTSF values varied between 10.10 and
 428 12.73, 10 and 12.29, and 13.23 and 13.97 for *Amapaí*, *Eucalyptus*, and *Miscanthus*,
 429 respectively, which is in line with the retained potassium degree and natural sensitivity
 430 of the biomass samples. Figure 5(d), (e), and (f), as well as Table 7 illustrate the obtained
 431 strong linear correlation ($0.918 < R^2 < 0.987$) between the CTSF and reaction rates and
 432 its statistical results. Comparing the calculated R^2 of the reaction rates correlation, the
 433 CTSF presented slightly better correlations than $K\%$ for *Amapaí* and *Eucalyptus*.
 434 Concerning *Miscanthus*, the CTSF was superior only for the k_{V_2} correlation. The results
 435 show that the expression $k_i = A \times CTSF + B$ (Table 7) provided statistically significant
 436 and accurate results. For instance, considering the applied potassium impregnation limits
 437 and explored biomasses, the CTSF can be used to predict the two-step reaction rates,
 438 which provides new insights and shows the usability of the operating condition-based
 439 index.

440 **Figure 5**

441 **Table 7**

442 3.4 Solid pseudo-component distribution

443 Figure 6 displays the solid A , B , and C , and volatile V_1 and V_2 pseudo-component
 444 evolution for *Amapaí* (a and b), *Eucalyptus* (c and d), and *Miscanthus* (e and f). Figures 7
 445 and 8 display solid and volatile pseudo-component contour mapping, enabling a complete
 446 assessment regarding the effect of the potassium content. The raw properties and $K\%$
 447 content impregnation (Tables 1 and 2), as well as the pre-exponential factors (Figures 3

448 and 4) and reaction rates (Table 3), assist the interpretation of the pseudo-component
449 evolution.

450 **Figure 6**

451 Considering that the torrefaction severity increases with potassium content, faster and
452 pronounced curves evidence the catalytic effect on the pseudo-component profiles, which
453 is consistent with [25,51,53]. The potassium impregnation's catalytic influence on
454 obtained solid product distribution is evidenced by an earlier and lower required time to
455 complete degradation of feedstock *A*, followed by the faster formation and lower final
456 values for intermediate solid *B*, and the earlier formation and higher final values of *C*
457 residue.

458 The complete degradation of *A* was evidenced with up to 20 min anticipation for
459 higher impregnation (0.009M). Figure 7 shows that *A* was fully consumed for
460 demineralized and impregnated samples within the torrefaction time range of 22–42min
461 for *Amapaí*, 25–37min for *Eucalyptus*, and 26–46min for *Miscanthus*, with lower times
462 for higher potassium content. This trend is in line with the kinetic rates (Figure 2) that
463 show faster k_1 for demineralized *Eucalyptus*, followed by *Amapaí* and *Miscanthus*.
464 Meanwhile, for impregnated samples, the faster k_1 was *Amapaí* > *Eucalyptus* >
465 *Miscanthus*.

466 **Figure 7**

467 The solid intermediated *B* presented lower final values for impregnated samples,
468 which varied between 6.6 and 40.0% for *Amapaí*, 18 and 47.8% for *Eucalyptus*, and 13.6
469 and 33.3% for *Miscanthus*. The catalytic behavior anticipated *B* peaks for impregnated
470 samples (0.009M) in 7 min for *Amapaí* and 6 min for both *Eucalyptus* and *Miscanthus*.

471 For *Amapaí* and *Miscanthus*, the demineralized residue *C* showed a small difference
472 compared to 0.003M experiments, followed by greater extents for 0.006M and 0.009M

473 treatments. C final values are in line with the $K\%$ content retained in biomass, with
474 variations of 28.28–38.43%, 14.57–26.83, and 26.06–32.27% for *Amapaí*, *Eucalyptus*,
475 and *Miscanthus*, respectively.

476 Regarding the literature on two-step reaction kinetics, Bach et al. (2016) applied the
477 model to evaluate torrefaction kinetics between 220 and 300 °C for spruce and birch
478 biomasses [51]. Additionally, Lin et al. (2019) conducted the numerical analysis for
479 poplar and fir torrefaction (200–230 °C) [25]. Moreover, Silveira et al. (2021) assessed
480 *Eucalyptus grandis* torrefaction kinetics between 210 and 290 °C [53]. The authors
481 reported that, for higher temperatures (higher torrefaction severity), the solid product
482 distribution for all analyzed biomasses showed faster degradation and formation for A , B ,
483 and C during torrefaction, in line with Figure 6.

484

485 3.5 Volatile pseudo-component distribution

486 Regarding the volatile pseudo-components (Figure 8), the potassium impact on the
487 behavior of volatile release was conditional to the K-loading amount, in agreement with
488 [25]. For the three biomasses, V_1 was released earlier, achieving earlier final constant
489 values for the impregnated samples. V_1 attempted constant final values for impregnated
490 and demineralized values between 19 and 35min for *Amapaí*, 23 and 32min for
491 *Eucalyptus*, and 23 and 41min for *Miscanthus*.

492

492 **Figure 8**

493 The higher $K(\%)$ containing samples had an earlier V_1 release than the demineralized
494 samples. Knowing that B formation occurs in parallel with V_1 release, the impregnated
495 samples (with earlier and pronounced B peaks) had lower or similar V_1 final yield
496 compared to the demineralized samples. Considering *Amapaí* and *Miscanthus*, V_1
497 presented an earlier release but lower final constant values for impregnated samples

498 compared to the demineralized ones. *Eucalyptus* presented equal or lower peaks for B ,
499 resulting in anticipated V_1 release, but similar final constant values.

500 The previous studies [26,32,81] showed a higher thermal reactivity for cellulose and
501 a consequent lower reactivity temperature, inducing an earlier decomposition with the
502 presence of potassium. Therefore, regarding the pseudo-component evolution (Figure 6),
503 the effect of potassium on the degradation kinetics in the second step reaction (formation
504 and release of C and V_2) is clear and could be scribed mainly for celluloses decomposition
505 [50].

506 A previous study [53] reported that the significance of V_2 increases with the
507 torrefaction severity and gains importance over V_1 for treatment above 275 °C, starting
508 its formation at roughly 30 min and is exclusive to the Severe (275–300 °C) treatments.
509 The potassium catalysis in V_2 is evidenced with its earlier release (roughly 10 min of
510 torrefaction) and the faster conversion for K-containing samples, following potassium
511 content.

512 The kinetics and product distribution obtained in the present analysis is consistent
513 with the conducted torrefaction experiments that evidenced higher CO and CO₂ yield
514 changes during the torrefaction experiment [32], highlighting that the noticeable growth
515 of V_2 with increased K content during the second step reaction properly represents the
516 catalytic effect. The results for the second step reaction and V_2 growth are in line with the
517 TG-FTIR results from [53], which showed an increase in CO and CO₂ release with
518 torrefaction severity.

519 Section 3.2 describes that *Amapai*, followed by *Miscanthus* and *Eucalyptus*, presented
520 higher reaction rates for the second step. This result is evidenced by the higher formation
521 of V_2 and C when comparing biomass species. The second volatile final values varied

522 from 15.5–43.7% for *Amapaí*, 19.6–38.2% for *Miscanthus*, and 19.7–37.6% for
523 *Eucalyptus*, which is in line with the K-containing content in the biomass samples.

524 4. Conclusion

525 The K_2CO_3 biomass impregnation influence on the 275 °C torrefaction kinetics was
526 investigated for *Amapaí*, *Eucalyptus*, and *Miscanthus* biomasses. The proposed PRNP
527 enables an accurate solid yield prediction ($R^2 > 0.9995$) that evaluates the induced catalytic
528 effect of potassium on kinetic degradation. The kinetic modeling with PRNP resulted in
529 unified activation energy values for the three biomasses and distinct pre-exponential
530 factors for each K% content. The numerical results showed faster reaction rates, lower
531 solid yields, and higher volatile yields, corroborating with the experimental results. A
532 strong R^2 (between 0.91 and 0.99) was obtained, as was a statically significant
533 ($p \leq 0.0463$) linear correlation for reaction rates and pre-exponential factor correlation
534 with $K\%$ for all three biomasses. The CTSF was calculated and provided a useful
535 performance indicator to predict kinetic parameters with slightly better linear
536 correlations than the $K\%$ content for the *Amapaí* and *Eucalyptus* biomasses. In
537 summary, the results are conducive to developing numerical models that consider fuel
538 flexibility and torrefaction performance for solid fuel upgrading under catalytic
539 conditions, while assessing the amount of recoverable and valuable volatiles.

540 Acknowledgments

541 This work was supported by the Brazilian National Council for Scientific and
542 Technological Development (CNPq), the French Agricultural Research Centre for
543 International Development (CIRAD) and the Brazilian Forest Products Laboratory.

544 References

545 [1] Lee S, Lo Y, Shen B, Dong W, Yong S, Akbar M, et al. Techno-economic
546 analysis for biomass supply chain : A state-of-the-art review. *Renew Sustain*

- 547 Energy Rev 2021;135:110164. <https://doi.org/10.1016/j.rser.2020.110164>.
- 548 [2] Cahyanti MN, Doddapaneni TRKC, Kikas T. Biomass torrefaction: An overview
549 on process parameters, economic and environmental aspects and recent
550 advancements. *Bioresour Technol* 2020;301:122737.
551 <https://doi.org/10.1016/j.biortech.2020.122737>.
- 552 [3] Ong HC, Chen WH, Singh Y, Gan YY, Chen CY, Show PL. A state-of-the-art
553 review on thermochemical conversion of biomass for biofuel production: A TG-
554 FTIR approach. *Energy Convers Manag* 2020;209:112634.
555 <https://doi.org/10.1016/j.enconman.2020.112634>.
- 556 [4] Mardhiah HH, Ong HC, Masjuki HH, Lim S, Pang YL. Investigation of carbon-
557 based solid acid catalyst from *Jatropha curcas* biomass in biodiesel production.
558 *Energy Convers Manag* 2017;144:10–7.
559 <https://doi.org/10.1016/j.enconman.2017.04.038>.
- 560 [5] Santanna MS, Silveira EA, Caldeira-Pires A. Thermochemical pathways for
561 municipal lignocellulosic waste as biofuel. 29th Eur. Biomass Conf. Exhib.,
562 2021. <https://doi.org/10.5071/29thEUBCE2021-3DV.6.8>.
- 563 [6] Zhang C, Ho SH, Chen WH, Xie Y, Liu Z, Chang JS. Torrefaction performance
564 and energy usage of biomass wastes and their correlations with torrefaction
565 severity index. *Appl Energy* 2018;220:598–604.
566 <https://doi.org/10.1016/j.apenergy.2018.03.129>.
- 567 [7] Chen W-H, Peng J, Bi XT. A state-of-the-art review of biomass torrefaction,
568 densification and applications. *Renew Sustain Energy Rev* 2015;44:847–66.
569 <https://doi.org/10.1016/j.rser.2014.12.039>.
- 570 [8] Chen W, Lin B, Lin Y, Chu Y, Ubando AT, Loke P, et al. Progress in biomass
571 torrefaction : Principles , applications and challenges. *Prog Energy Combust Sci*
572 2021;82:100887. <https://doi.org/10.1016/j.pecs.2020.100887>.
- 573 [9] Kumar R, Sarkar A, Prasad J. Effect of torrefaction on the physicochemical
574 properties of eucalyptus derived biofuels : estimation of kinetic parameters and
575 optimizing torrefaction using response surface methodology (RSM). *Energy*
576 2020;198:117369. <https://doi.org/10.1016/j.energy.2020.117369>.
- 577 [10] Santanna MS, Silveira EA, Macedo L, Galvão LGO, Caldeira-Pires A.
578 Torrefaction of lignocellulosic municipal solid waste: thermal upgrade for energy
579 use. 28th Eur. Biomass Conf. Exhib., Marseille: 2020, p. 188–91.
580 <https://doi.org/10.5071/28thEUBCE2020-1DV.1.34>.
- 581 [11] da Silva JCG, Pereira JLC, Andersen SLF, Moreira R de FPM, José HJ.
582 Torrefaction of ponkan peel waste in tubular fixed-bed reactor: In-depth
583 bioenergetic evaluation of torrefaction products. *Energy* 2020;210.
584 <https://doi.org/10.1016/j.energy.2020.118569>.
- 585 [12] Yan B, Jiao L, Li J, Zhu X, Ahmed S, Chen G. Investigation on microwave
586 torrefaction: Parametric influence, TG-MS-FTIR analysis, and gasification
587 performance. *Energy* 2021;220. <https://doi.org/10.1016/j.energy.2021.119794>.
- 588 [13] Riva L, Wang L, Ravenni G, Bartocci P, Videm T, Skreiberg Ø, et al.
589 Considerations on factors affecting biochar densification behavior based on a

- 590 multiparameter model. *Energy* 2021;221:119893.
591 <https://doi.org/10.1016/j.energy.2021.119893>.
- 592 [14] Arriola E, Chen W, Chih Y, Daniel M, Luna D. Impact of post-torrefaction
593 process on biochar formation from wood pellets and self-heating phenomena for
594 production safety. *Energy* 2020;207:118324.
595 <https://doi.org/10.1016/j.energy.2020.118324>.
- 596 [15] Basu P. *Biomass Gasification, Pyrolysis and Torrefaction Practical Design and*
597 *Theory*. 3rd Editio. 2018. <https://doi.org/10.1016/C2016-0-04056-1>.
- 598 [16] Chen WH, Kuo PC. Torrefaction and co-torrefaction characterization of
599 hemicellulose, cellulose and lignin as well as torrefaction of some basic
600 constituents in biomass. *Energy* 2011;36:803–11.
601 <https://doi.org/10.1016/j.energy.2010.12.036>.
- 602 [17] Homem De Faria Bruno DF, Charline L, Jeremy V, Patrick R, Oliveira Carneiro
603 Angélica DC, Armando CP, et al. Emulation of field storage conditions for
604 assessment of energy properties of torrefied sugarcane bagasses. *Biomass and*
605 *Bioenergy* 2021;145. <https://doi.org/10.1016/j.biombioe.2020.105938>.
- 606 [18] Commandré JM, Leboeuf A. Volatile yields and solid grindability after
607 torrefaction of various biomass types. *Environ Prog Sustain Energy*
608 2015;34:1180–6. <https://doi.org/10.1002/ep.12073>.
- 609 [19] Thengane SK, Kung KS, Gupta A, Ateia M, Sanchez DL, Mahajani SM, et al.
610 Oxidative torrefaction for cleaner utilization of biomass for soil amendment.
611 *Clean Eng Technol* 2020;1:100033. <https://doi.org/10.1016/j.clet.2020.100033>.
- 612 [20] Sher F, Yaqoob A, Saeed F, Zhang S, Jahan Z, Klemeš JJ. Torrefied biomass
613 fuels as a renewable alternative to coal in co-firing for power generation. *Energy*
614 2020;209. <https://doi.org/10.1016/j.energy.2020.118444>.
- 615 [21] Nguyen NM, Alobaid F, May J, Peters J, Epple B. Experimental study on steam
616 gasification of torrefied woodchips in a bubbling fluidized bed reactor. *Energy*
617 2020;202. <https://doi.org/10.1016/j.energy.2020.117744>.
- 618 [22] Zheng A, Li L, Tippayawong N, Huang Z. Reducing emission of NO_x and SO_x
619 precursors while enhancing char production from pyrolysis of sewage sludge by
620 torrefaction pretreatment. *Energy* 2020;192:116620.
621 <https://doi.org/10.1016/j.energy.2019.116620>.
- 622 [23] Silveira EA, Morais MVG de, Rousset P, Caldeira-Pires A, Pétrissans A, Galvão
623 LGO. Coupling of an acoustic emissions system to a laboratory torrefaction
624 reactor. *J Anal Appl Pyrolysis* 2018;129:29–36.
625 <https://doi.org/10.1016/j.jaap.2017.12.008>.
- 626 [24] Khazraie Shoulaifar T, Demartini N, Karlström O, Hupa M. Impact of
627 organically bonded potassium on torrefaction: Part 1. Experimental. *Fuel*
628 2016;165:544–52. <https://doi.org/10.1016/j.fuel.2015.06.024>.
- 629 [25] Lin B-J, Silveira EA, Colin B, Chen W-H, Lin Y-Y, Leconte F, et al. Modeling
630 and prediction of devolatilization and elemental composition of wood during
631 mild pyrolysis in a pilot-scale reactor. *Ind Crops Prod* 2019;131:357–70.
632 <https://doi.org/10.1016/j.indcrop.2019.01.065>.

- 633 [26] Khazraie Shoulafar T, Demartini N, Karlström O, Hemming J, Hupa M. Impact
634 of organically bonded alkali metals on torrefaction: Part 2. Modeling. *Fuel*
635 2016;168:107–15. <https://doi.org/10.1016/j.fuel.2015.11.084>.
- 636 [27] Barta-Rajnai E, Babinszki B, Sebestyén Z, Czirok SI, May Z, Jakab E, et al. On
637 the significance of potassium and chlorine content of lignocellulose during
638 torrefaction. *J Anal Appl Pyrolysis* 2018;135:32–43.
639 <https://doi.org/10.1016/j.jaap.2018.09.024>.
- 640 [28] MACEDO LA DE. Torréfaction de biomasse lignocellulosique : effet catalytique
641 du potassium sur les espèces condensables. UNIVERSITÉ DE LORRAINE,
642 2017.
- 643 [29] Macedo LA de, Silveira EA, Commandré J-M, Rousset P, Valette J, Pétrissans
644 M. Biomass Potassium Impregnation Effect on Oxidative Torrefaction. 29th Eur.
645 Biomass Conf. Exhib., 2021. [https://doi.org/10.5071/29thEUBCE2021-](https://doi.org/10.5071/29thEUBCE2021-3DV.6.12)
646 3DV.6.12.
- 647 [30] Silveira EA, Macedo LA, Candelier K, Rousset P, Commandré J-M. Assessment
648 of catalytic torrefaction promoted by biomass potassium impregnation through
649 performance indexes. *Fuel* 2021. <https://doi.org/10.1016/j.fuel.2021.121353>.
- 650 [31] Liu X, Yi C, Chen L, Niu R, Mi T, Wu Q, et al. Synergy of steam reforming and
651 K₂CO₃ modification on wood biomass pyrolysis. *Cellulose* 2019;26:6049–60.
652 <https://doi.org/10.1007/s10570-019-02480-3>.
- 653 [32] Macedo LA de, Commandré JM, Rousset P, Valette J, Pétrissans M. Influence of
654 potassium carbonate addition on the condensable species released during wood
655 torrefaction. *Fuel Process Technol* 2018;169:248–57.
656 <https://doi.org/10.1016/j.fuproc.2017.10.012>.
- 657 [33] Ong HC, Chen WH, Farooq A, Gan YY, Lee KT, Ashokkumar V. Catalytic
658 thermochemical conversion of biomass for biofuel production: A comprehensive
659 review. *Renew Sustain Energy Rev* 2019;113:109266.
660 <https://doi.org/10.1016/j.rser.2019.109266>.
- 661 [34] Safar M, Lin B-JJ, Chen W-HH, Langauer D, Chang J-SS, Raclavska H, et al.
662 Catalytic effects of potassium on biomass pyrolysis, combustion and torrefaction.
663 *Appl Energy* 2019;235:346–55. <https://doi.org/10.1016/j.apenergy.2018.10.065>.
- 664 [35] Shen Y, Zhang N, Zhang S. Catalytic pyrolysis of biomass with potassium
665 compounds for Co-production of high-quality biofuels and porous carbons.
666 *Energy* 2020;190:116431. <https://doi.org/10.1016/j.energy.2019.116431>.
- 667 [36] Wang Z, Wang F, Cao J, Wang J. Pyrolysis of pine wood in a slowly heating
668 fixed-bed reactor: Potassium carbonate versus calcium hydroxide as a catalyst.
669 *Fuel Process Technol* 2010;91:942–50.
670 <https://doi.org/10.1016/j.fuproc.2009.09.015>.
- 671 [37] Zhang S, Su Y, Ding K, Zhang H. Impacts and release characteristics of K and
672 Mg contained in rice husk during torrefaction process. *Energy* 2019;186:115888.
673 <https://doi.org/10.1016/j.energy.2019.115888>.
- 674 [38] Zhang S, Su Y, Ding K, Zhu S, Zhang H, Liu X, et al. Effect of inorganic species
675 on torrefaction process and product properties of rice husk. *Bioresour Technol*

- 676 2018;265:450–5. <https://doi.org/10.1016/j.biortech.2018.06.042>.
- 677 [39] Cheol K, Kim J, Yong S, Jun S, Hoon L, Geon C, et al. Development and
678 validation of torrefaction optimization model applied element content prediction
679 of biomass. *Energy* 2021;214:119027.
680 <https://doi.org/10.1016/j.energy.2020.119027>.
- 681 [40] Zhang Z, Duan H, Zhang Y, Guo X, Yu X, Zhang X, et al. Investigation of
682 kinetic compensation effect in lignocellulosic biomass torrefaction: Kinetic and
683 thermodynamic analyses. *Energy* 2020;207.
684 <https://doi.org/10.1016/j.energy.2020.118290>.
- 685 [41] Duan H, Zhang Z, Rahman M, Guo X, Zhang X, Cai J. Insight into torrefaction
686 of woody biomass : Kinetic modeling using pattern search method. *Energy*
687 2020;201:117648. <https://doi.org/10.1016/j.energy.2020.117648>.
- 688 [42] Silveira EA, Lin BJ, Colin B, Chaouch M, Pétrissans A, Rousset P, et al. Heat
689 treatment kinetics using three-stage approach for sustainable wood material
690 production. *Ind Crops Prod* 2018;124:563–71.
691 <https://doi.org/10.1016/j.indcrop.2018.07.045>.
- 692 [43] Lin B-J, Silveira EA, Colin B, Chen W-H, Pétrissans A, Rousset P, et al.
693 Prediction of higher heating values (HHVs) and energy yield during torrefaction
694 via kinetics. *Energy Procedia* 2019;158:111–6.
695 <https://doi.org/10.1016/j.egypro.2019.01.054>.
- 696 [44] Silveira EA, Macedo L, Rousset P, Commandré J-M, Galvão LGO, Chaves BS.
697 The effect of potassium carbonate wood impregnation on torrefaction kinetics.
698 29th Eur. Biomass Conf. Exhib., 2021. <https://doi.org/10.5071/29thEUBCE2021-3DV.6.4>.
- 700 [45] Chen WH, Kuo PC. Isothermal torrefaction kinetics of hemicellulose, cellulose,
701 lignin and xylan using thermogravimetric analysis. *Energy* 2011;36:6451–60.
702 <https://doi.org/10.1016/j.energy.2011.09.022>.
- 703 [46] Chen WH, Wu ZY, Chang JS. Isothermal and non-isothermal torrefaction
704 characteristics and kinetics of microalga *Scenedesmus obliquus* CNW-N.
705 *Bioresour Technol* 2014;155:245–51.
706 <https://doi.org/10.1016/j.biortech.2013.12.116>.
- 707 [47] Shang L, Ahrenfeldt J, Holm JK, Barsberg SS, Zhang RZ, Luo YH, et al.
708 Intrinsic kinetics and devolatilization of wheat straw during torrefaction. *J Anal*
709 *Appl Pyrolysis* 2013;100:145–52. <https://doi.org/10.1016/j.jaap.2012.12.010>.
- 710 [48] Gul S, Ramzan N, Hanif MA, Bano S. Kinetic, volatile release modeling and
711 optimization of torrefaction. *J Anal Appl Pyrolysis* 2017;128:44–53.
712 <https://doi.org/10.1016/j.jaap.2017.11.001>.
- 713 [49] Di Blasi C, Lanzetta M. Intrinsic kinetics of isothermal xylan degradation in inert
714 atmosphere. *J Anal Appl Pyrolysis* 1997;40–41:287–303.
715 [https://doi.org/10.1016/S0165-2370\(97\)00028-4](https://doi.org/10.1016/S0165-2370(97)00028-4).
- 716 [50] Bates RB, Ghoniem AF. Biomass torrefaction: Modeling of volatile and solid
717 product evolution kinetics. *Bioresour Technol* 2012;124:460–9.
718 <https://doi.org/10.1016/j.biortech.2012.07.018>.

- 719 [51] Bach QV, Chen WH, Chu YS, Skreiberg ??yvind, Skreiberg Ø. Predictions of
720 biochar yield and elemental composition during torrefaction of forest residues.
721 Bioresour Technol 2016;215:239–46.
722 <https://doi.org/10.1016/j.biortech.2016.04.009>.
- 723 [52] Silveira EA, Oliveira Galvão LG, Alves de Macedo L, A. Sá I, S. Chaves B,
724 Girão de Moraes MV, et al. Thermo-Acoustic Catalytic Effect on Oxidizing
725 Woody Torrefaction. Processes 2020;8:1361. <https://doi.org/10.3390/pr8111361>.
- 726 [53] Silveira EA, Luz SM, Leão RM, Rousset P, Caldeira-Pires A. Numerical
727 modeling and experimental assessment of sustainable woody biomass
728 torrefaction via coupled TG-FTIR. Biomass and Bioenergy 2021;146:105981.
729 <https://doi.org/10.1016/j.biombioe.2021.105981>.
- 730 [54] Cavagnol S, Sanz E, Nastoll W, Roesler J, Zymly V, Perré P. Inverse analysis of
731 wood pyrolysis with long residence times in the temperature range 210–290°C:
732 Selection of multi-step kinetic models based on mass loss residues. Thermochim
733 Acta 2013;574:1–9.
- 734 [55] Klinger J, Klemetsrud B, Bar-Ziv E, Shonnard D. Temperature dependence of
735 aspen torrefaction kinetics. J Anal Appl Pyrolysis 2014;110:424–9.
736 <https://doi.org/10.1016/j.jaap.2014.10.008>.
- 737 [56] Branca C., Di Blasi C. Kinetics of the isothermal degradation of wood in the
738 temperature range 528-708K. J Anal Appl Pyrolysis 2003;67:207–19.
- 739 [57] Rousset P, Turner I, Donnot A, Perré P. Choix d'un modèle de pyrolyse ménagée
740 du bois à l'échelle de la microparticule en vue de la modélisation macroscopique.
741 Ann For Sci 2006;63:213–29. <https://doi.org/10.1051/forest:2005113>.
- 742 [58] Trubetskaya A, Surup G, Shapiro A, Bates RB. Modeling the influence of
743 potassium content and heating rate on biomass pyrolysis. Appl Energy
744 2017;194:199–211. <https://doi.org/10.1016/j.apenergy.2017.03.009>.
- 745 [59] Turner I, Rousset P, Rémond R, Perré P. An experimental and theoretical
746 investigation of the thermal treatment of wood (*Fagus sylvatica* L.) in the range
747 200-260 °C. Int J Heat Mass Transf 2010;53:715–25.
748 <https://doi.org/10.1016/j.ijheatmasstransfer.2009.10.020>.
- 749 [60] Guo F, Liu Y, Wang Y, Li X, Li T, Guo C. Pyrolysis kinetics and behavior of
750 potassium-impregnated pine wood in TGA and a fixed-bed reactor. Energy
751 Convers Manag 2016;130:184–91.
752 <https://doi.org/10.1016/j.enconman.2016.10.055>.
- 753 [61] Lin YY, Chen WH, Colin B, Lin BJ, Leconte F, Pétrissans A, et al. Pyrolysis
754 kinetics of potassium-impregnated rubberwood analyzed by evolutionary
755 computation. Bioresour Technol 2021;319.
756 <https://doi.org/10.1016/j.biortech.2020.124145>.
- 757 [62] Bates RB, Ghoniem AF. Biomass torrefaction: modeling of reaction
758 thermochemistry. Bioresour Technol 2013;134:331–40.
759 <https://doi.org/10.1016/j.biortech.2013.01.158>.
- 760 [63] Bates RB, Ghoniem AF. Modeling kinetics-transport interactions during biomass
761 torrefaction: The effects of temperature, particle size, and moisture content. Fuel

- 762 2014;137:216–29. <https://doi.org/10.1016/j.fuel.2014.07.047>.
- 763 [64] Silveira EA, Luz S, Santanna MS, Leão RM, Rousset P, Pires AC-. Thermal
764 upgrading of sustainable woody material: experimental and numerical
765 torrefaction assessment. 28th Eur. Biomass Conf. Exhib., Virtual: 2020, p. 694–
766 8. <https://doi.org/10.5071/28thEUBCE2020-3CV.2.5>.
- 767 [65] Galvão LGOBSC, Morais MVG de, Vale AT do V, Caldeira-Pires A, Rousset P,
768 Silveira EA. Combined thermo-acoustic upgrading of solid fuel: experimental
769 and numerical investigation. 28th Eur. Biomass Conf. Exhib., 2020, p. 6–9.
- 770 [66] Abraf. Anuário Estatístico-Associação Brasileira de Produtores de Florestas
771 Plantadas. Anuário Estatístico ABRAF 2013:146.
- 772 [67] Silveira EA, Galvão LGO, Sá IA, Silva BF, Macedo L, Rousset P, et al. Effect of
773 torrefaction on thermal behavior and fuel properties of Eucalyptus grandis macro-
774 particulates. J Therm Anal Calorim 2019;138:3645–52.
775 <https://doi.org/10.1007/s10973-018-07999-4>.
- 776 [68] Chung J-H, Kim D-S. Miscanthus as a potential bioenergy crop in East Asia. J
777 Crop Sci Biotechnol 2012;15:65–77. <https://doi.org/10.1007/s12892-012-0023-0>.
- 778 [69] Van de steene L, Tagutchou JP, Escudero Sanz FJ, Salvador S. Gasification of
779 woodchip particles: Experimental and numerical study of char-H₂O, char-CO₂,
780 and char-O₂ reactions. Chem Eng Sci 2011;66:4499–509.
781 <https://doi.org/10.1016/j.ces.2011.05.045>.
- 782 [70] Daouk E, Van de Steene L, Paviet F, Salvador S. Thick wood particle pyrolysis
783 in an oxidative atmosphere. Chem Eng Sci 2015;126:608–15.
784 <https://doi.org/10.1016/j.ces.2015.01.017>.
- 785 [71] Noumi ES, Blin J, Valette J, Rousset P. Combined Effect of Pyrolysis Pressure
786 and Temperature on the Yield and CO₂ Gasification Reactivity of Acacia Wood
787 in macro-TG. Energy & Fuels 2015;29:7301–8.
788 <https://doi.org/10.1021/acs.energyfuels.5b01454>.
- 789 [72] Chaves BS, Macedo LA, Galvão LGO, Carvalho ACR, Palhano AX, Vale AT, et
790 al. Production and characterization of raw and torrefied phyllostachys aurea
791 pellets and briquettes for energy purposes. 29th Eur. Biomass Conf. Exhib., 2021,
792 p. 657–61. <https://doi.org/10.5071/29thEUBCE2021-2DV.2.1>.
- 793 [73] Silveira EA, Luz S, Candelier K, Macedo LA, Rousset P. An assessment of
794 biomass torrefaction severity indexes. Fuel 2021;288:119631.
795 <https://doi.org/10.1016/j.fuel.2020.119631>.
- 796 [74] Chen WH, Cheng CL, Show PL, Ong HC. Torrefaction performance prediction
797 approached by torrefaction severity factor. Fuel 2019;251:126–35.
798 <https://doi.org/10.1016/j.fuel.2019.04.047>.
- 799 [75] Silveira EA, Macedo L, Commandré J-M, Candelier K, Rousset P. Potassium
800 Impregnation Assessment of Mild Biomass Pyrolysis by Catalytic Torrefaction
801 Severity Factor. 29th Eur. Biomass Conf. Exhib., 2021, p. 1015–9.
802 <https://doi.org/10.5071/29thEUBCE2021-3DV.6.5>.
- 803 [76] Iftikhar M, Asghar A, Ramzan N, Sajjadi B, Chen W. Biomass densification:
804 Effect of cow dung on the physicochemical properties of wheat straw and rice

- 805 husk based biomass pellets. J 2019;122.
806 <https://doi.org/10.1016/j.biombioe.2019.01.005>.
- 807 [77] Shang L, Ahrenfeldt J, Holm JK, Bach LS, Stelte W, Henriksen UB. Kinetic
808 model for torrefaction of wood chips in a pilot-scale continuous reactor. J Anal
809 Appl Pyrolysis 2014;108:109–16. <https://doi.org/10.1016/j.jaap.2014.05.010>.
- 810 [78] Prins MJ, Ptasinski KJ, Janssen FJJG. Torrefaction of wood. Part 1. Weight loss
811 kinetics. J Anal Appl Pyrolysis 2006;77:28–34.
812 <https://doi.org/10.1016/j.jaap.2006.01.002>.
- 813 [79] Shimada N, Kawamoto H, Saka S. Different action of alkali/alkaline earth metal
814 chlorides on cellulose pyrolysis. J Anal Appl Pyrolysis 2008;81:80–7.
815 <https://doi.org/10.1016/j.jaap.2007.09.005>.
- 816 [80] Xing S, Yuan H, Huhetaoli, Qi Y, Lv P, Yuan Z, et al. Characterization of the
817 decomposition behaviors of catalytic pyrolysis of wood using copper and
818 potassium over thermogravimetric and Py-GC/MS analysis. Energy
819 2016;114:634–46. <https://doi.org/10.1016/j.energy.2016.07.154>.
- 820 [81] Chen WH, Fong Eng C, Lin YY, Bach QV, Ashokkumar V, Show PL. Two-step
821 thermodegradation kinetics of cellulose, hemicelluloses, and lignin under
822 isothermal torrefaction analyzed by particle swarm optimization. Energy Convers
823 Manag 2021;238:114116. <https://doi.org/10.1016/j.enconman.2021.114116>.
- 824
825
826
827
828
829
830
831
832
833
834
835
836
837
838
839
840

841 **Table 1.** Chemical composition (in %, in dry basis) of raw *Amapaí*, *Eucalyptus* [28,32]
 842 and *Miscanthus* [28] biomasses by proximate, fiber, ultimate and mineral analyses.

| Feedstock | <i>Amapaí</i> | <i>Eucalyptus</i> | <i>Miscanthus</i> |
|---|--------------------------------------|--------------------------------------|--------------------------------------|
| Proximate analysis | | | |
| Ash | 0.85 | 0.35 | 2.91 |
| Fiber analysis | | | |
| Hemicelluloses | 11.3 | 13.7 | 27.7 |
| Cellulose | 51.2 | 58.6 | 45.0 |
| Lignin | 30.4 | 19.4 | 11.4 |
| Other | 7.1 | 8.3 | 15.9 |
| Ultimate analysis | | | |
| C | 51.01 | 49.96 | 48.56 |
| H | 5.78 | 5.60 | 5.73 |
| N | 0.23 | 0.13 | 0.22 |
| O ^a | 42.13 | 43.97 | 42.57 |
| Chemical formula | CH _{1.36} O _{0.62} | CH _{1.35} O _{0.66} | CH _{1.42} O _{0.66} |
| HHV (MJ kg⁻¹)^b | 20.03 | 19.63 | 19.24 |
| Inorganic elements by ICP-AES | | | |
| K | 0.086 | 0.027 | 0.379 |
| Na | 0.026 | 0.012 | 0.013 |
| P | 0.014 | 0.003 | 0.0320 |
| Ca | 0.179 | <DL ^c | 0.276 |

843 ^aBy difference O = 100 – (C + H + N + ash), ^bCalculate [25], ^cDL: detection limit.

844

845

846

847

848

849 **Table 2.** K content (in %, dry basis) in demineralized and impregnated *Amapaí*,
 850 *Eucalyptus* and *Miscanthus* biomasses, issued from ICP-AES analyses [32].

| Species | K(%) ^a |
|---------------------------------------|-------------------|
| <i>Amapaí</i> | |
| Demineralized | 0.011 |
| 0.003M K ₂ CO ₃ | 0.229 |
| 0.006M K ₂ CO ₃ | 0.314 |
| 0.009M K ₂ CO ₃ | 0.527 |
| <i>Eucalyptus</i> | |
| Demineralized | 0.009 |
| 0.003M K ₂ CO ₃ | 0.149 |
| 0.006M K ₂ CO ₃ | 0.253 |
| 0.009M K ₂ CO ₃ | 0.387 |
| <i>Miscanthus</i> | |
| Demineralized | 0.017 |
| 0.003M K ₂ CO ₃ | 0.182 |
| 0.006M K ₂ CO ₃ | 0.280 |
| 0.009M K ₂ CO ₃ | 0.403 |

851 ^a dry basis

852

853

854

855

856

857

858

859

860

861

862

863

864

865

866 **Table 3.** Kinetic parameters obtained with the PRNP, according to the biomass species
 867 and their potassium concentrations.

| Species | Reaction | | $A \rightarrow B$ | $A \rightarrow V_1$ | $B \rightarrow C$ | $B \rightarrow V_2$ | R^2 |
|-------------------|----------------------------|----------|-------------------|---------------------|-------------------|---------------------|--------|
| | Kinetic constant | E_{ai} | k_1 | k_{V_1} | k_2 | k_{V_2} | |
| | Concentration in K_2CO_3 | | 82307.09 | 149275.20 | 35491.09 | 124583.90 | |
| <i>Amapaí</i> | Dem. | A_{oi} | 1.73E+07 | 1.27E+13 | 2.10E+01 | 3.72E+09 | 0.9995 |
| | 0.003M | | 3.06E+07 | 2.06E+13 | 2.58E+01 | 1.10E+10 | 0.9998 |
| | 0.006M | | 3.64E+07 | 2.96E+13 | 3.52E+01 | 1.39E+10 | 0.9999 |
| | 0.009M | | 4.73E+07 | 3.39E+13 | 4.97E+01 | 1.95E+10 | 0.9999 |
| <i>Eucalyptus</i> | Dem. | A_{oi} | 1.99E+07 | 1.79E+13 | 1.02E+01 | 4.74E+09 | 0.9999 |
| | 0.003M | | 2.56E+07 | 2.54E+13 | 1.88E+01 | 7.47E+09 | 0.9999 |
| | 0.006M | | 3.40E+07 | 3.61E+13 | 2.28E+01 | 1.03E+10 | 0.9998 |
| | 0.009M | | 3.66E+07 | 4.12E+13 | 2.71E+01 | 1.34E+10 | 0.9998 |
| <i>Miscanthus</i> | Dem. | A_{oi} | 1.39E+07 | 1.35E+13 | 2.20E+01 | 5.32E+09 | 0.9998 |
| | 0.003M | | 1.93E+07 | 1.84E+13 | 2.48E+01 | 8.05E+09 | 0.9999 |
| | 0.006M | | 2.67E+07 | 2.12E+13 | 3.04E+01 | 1.20E+10 | 0.9998 |
| | 0.009M | | 3.37E+07 | 3.18E+13 | 3.48E+01 | 1.38E+10 | 0.9997 |

868 E_{ai} : Activation energies ($J.mol^{-1}$); A_{oi} : pre-exponential factors (min^{-1}) ($i = 1, 2, V_1$ and V_2).

869

870

871

872

873

874

875

876

877

878

879

880

881

882

883 **Table 4.** Correlation statistics between reaction rates and the potassium content K (%) for
 884 *Amapaí*, *Eucalyptus*, and *Miscanthus*. The curve fit is of the form $k_i = A \times K(\%) + B$.

| | Reaction rate | Correlation coef. (R_{CC}) ^a | p-Value | A | B | R^2 |
|-------------------|---------------|---|---------|----------|-----------|--------|
| <i>Amapaí</i> | k_1 | 0.9791 | 0.0021* | 1.96E+00 | -1.34E+00 | 0.9586 |
| | k_{V_1} | 0.9578 | 0.0041* | 1.97E+00 | -2.54E+00 | 0.9174 |
| | k_2 | 0.9765 | 0.0235* | 1.72E+00 | -4.81E+00 | 0.9535 |
| | k_{V_2} | 0.9548 | 0.0045* | 3.20E+00 | -5.15E+00 | 0.9117 |
| <i>Eucalyptus</i> | k_1 | 0.9711 | 0.0289* | 1.69E+00 | -1.24E+00 | 0.9429 |
| | k_{V_1} | 0.9790 | 0.0209* | 2.29+00 | -2.22E+00 | 0.9585 |
| | k_2 | 0.9552 | 0.0448* | 2.53E+00 | -5.37E+00 | 0.9124 |
| | k_{V_2} | 0.9928 | 0.0072* | 2.77E+00 | -5.04E+00 | 0.9857 |
| <i>Miscanthus</i> | k_1 | 0.9949 | 0.0051* | 2.35E+00 | -1.66E+00 | 0.9897 |
| | k_{V_1} | 0.9847 | 0.0152* | 2.16E+00 | -2.59E+00 | 0.9697 |
| | k_2 | 0.9819 | 0.0181* | 1.24E+00 | -4.74E+00 | 0.9641 |
| | k_{V_2} | 0.9827 | 0.0173* | 2.59E+00 | -4.97E+00 | 0.9657 |

885 * Denotes statistically significant p-values, ^a linear correlation coefficient.

886

887

888

889

890

891

892

893

894

895

896

897

898

899

900

901

902

903 **Table 5.** Correlation statistics between pre-exponential factor A_0i (min^{-1}) and the
 904 potassium content $K(\%)$ for *Amapaí*, *Eucalyptus*, and *Miscanthus*. The curve fit is of the
 905 form $A_0i = A \times K(\%) + B$.

| | Reaction | Correlation coef. (R_{CC}) ^a | p-Value | A | B | R^2 |
|-------------------|---------------------|--|---------|----------|----------|--------|
| <i>Amapaí</i> | $A \rightarrow B$ | 0.9983 | 0.0016* | 5.85E+07 | 1.71E+07 | 0.9968 |
| | $A \rightarrow V_1$ | 0.9675 | 0.0325* | 4.29E+13 | 1.26E+13 | 0.9359 |
| | $B \rightarrow C$ | 0.9617 | 0.0383* | 5.69E+01 | 1.75E+01 | 0.9249 |
| <i>Eucalyptus</i> | $B \rightarrow V_2$ | 0.9973 | 0.0027* | 3.07E+10 | 3.76E+09 | 0.9946 |
| | $A \rightarrow B$ | 0.9749 | 0.0251* | 4.67E+07 | 1.97E+07 | 0.9504 |
| | $A \rightarrow V_1$ | 0.9856 | 0.0144* | 6.46E+13 | 1.73E+13 | 0.9713 |
| | $B \rightarrow C$ | 0.9858 | 0.0141* | 4.42E+01 | 1.09E+01 | 0.9719 |
| <i>Miscanthus</i> | $B \rightarrow V_2$ | 0.9982 | 0.0018* | 2.31E+10 | 4.36E+09 | 0.9963 |
| | $A \rightarrow B$ | 0.9857 | 0.0142* | 5.22E+07 | 1.19E+07 | 0.9717 |
| | $A \rightarrow V_1$ | 0.9537 | 0.0463* | 4.54E+13 | 1.12E+13 | 0.9095 |
| | $B \rightarrow C$ | 0.9752 | 0.0247* | 3.43E+01 | 2.04E+01 | 0.9511 |
| | $B \rightarrow V_2$ | 0.9822 | 0.0178* | 2.30E+10 | 4.71E+09 | 0.9646 |

906 * Denotes statistically significant p-values, ^a linear correlation coefficient.

907

908

909

910

911

912

913

914

915

916

917

918

919

920

921 **Table 6.** CTSF and α_{cat} according to the biomass species and potassium concentrations.

| | <i>Amapaí</i> | <i>Eucalyptus</i> | <i>Miscanthus</i> |
|----------------|---------------|-------------------|-------------------|
| α_{cat} | 2.0 | 1.9 | 2.8 |
| Demineralized | 11.76 | 11.58 | 13.23 |
| 0.003M | 12.18 | 11.85 | 13.56 |
| 0.006M | 12.34 | 12.04 | 13.74 |
| 0.009M | 12.73 | 12.29 | 13.97 |

922

923

924

925

926

927

928

929

930

931

932

933

934

935

936

937

938

939

940

941 **Table 7.** Correlation statistics between reaction rates and the CTSF for *Amapaí*,
 942 *Eucalyptus*, and *Miscanthus*. The curve fit is of the form
 943 $k_i = A \times CTSF + B$.

| | Reaction rate | Correlation coef. (R_{CC}) ^a | p-Value | A | B | R^2 |
|-------------------|---------------|---|---------|------|--------|--------|
| <i>Amapaí</i> | k_1 | 0.9819 | 0.0180* | 1.04 | -13.61 | 0.9643 |
| | k_{V_1} | 0.9610 | 0.0389* | 1.05 | -14.91 | 0.9236 |
| | k_2 | 0.9746 | 0.0253* | 0.91 | -15.52 | 0.9500 |
| | k_{V_2} | 0.9591 | 0.0408* | 1.71 | -25.26 | 0.9199 |
| <i>Eucalyptus</i> | k_1 | 0.9713 | 0.0287* | 0.90 | -11.67 | 0.9434 |
| | k_{V_1} | 0.9794 | 0.0205* | 1.23 | -16.38 | 0.9593 |
| | k_2 | 0.9580 | 0.0419* | 1.35 | -21.01 | 0.9178 |
| | k_{V_2} | 0.9935 | 0.0065* | 1.47 | -22.15 | 0.9870 |
| <i>Miscanthus</i> | k_1 | 0.9935 | 0.0064* | 1.23 | -17.84 | 0.9871 |
| | k_{V_1} | 0.9826 | 0.0174* | 1.24 | -17.43 | 0.9655 |
| | k_2 | 0.9783 | 0.0217* | 0.64 | -13.24 | 0.9571 |
| | k_{V_2} | 0.9831 | 0.0169* | 1.35 | -22.79 | 0.9664 |

944 * Denotes statistically significant p-values, ^a linear correlation coefficient.

945

946

947

948

949

950

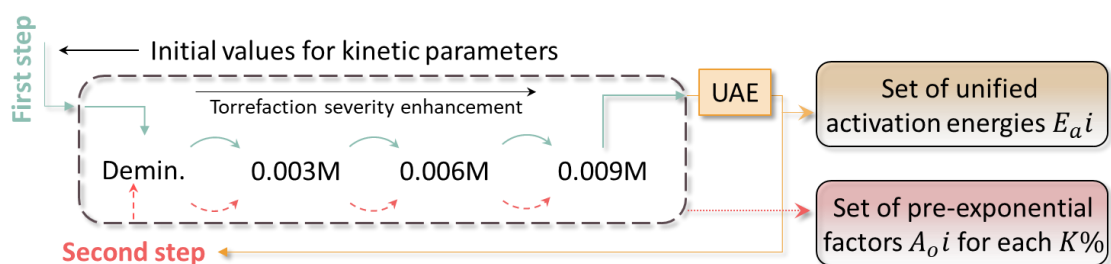
951

952

953

954

955



956

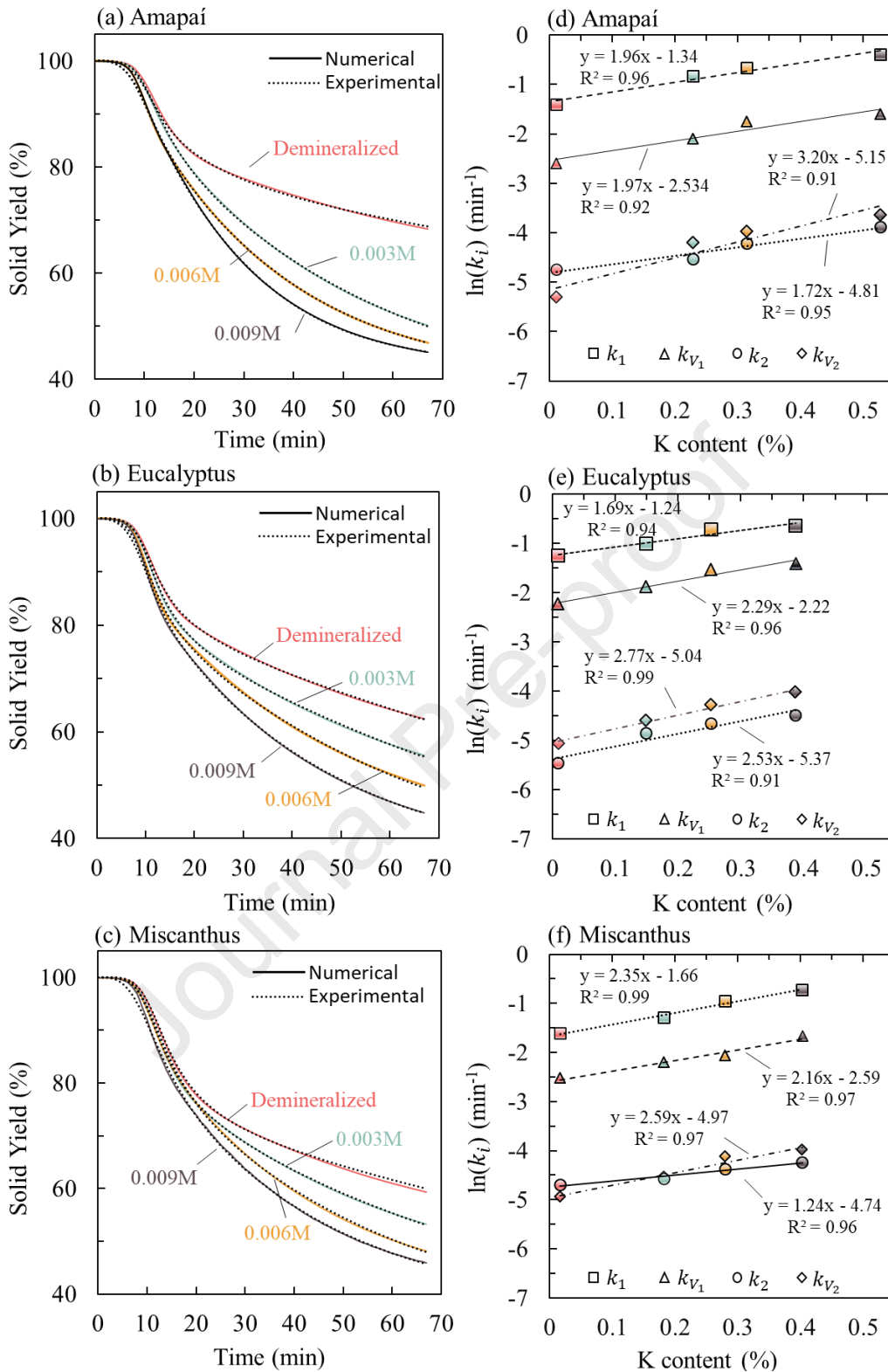
957 **Figure 01.** Methodology for the potassium responsive numerical path (PRNP). E_{ai}
 958 Activation energies ($\text{kJ}\cdot\text{mol}^{-1}$); A_{oi} pre-exponential factors (min^{-1}) ($i =$
 959 $1, 2, V_1$ and V_2). (2-column fitting)

960

961

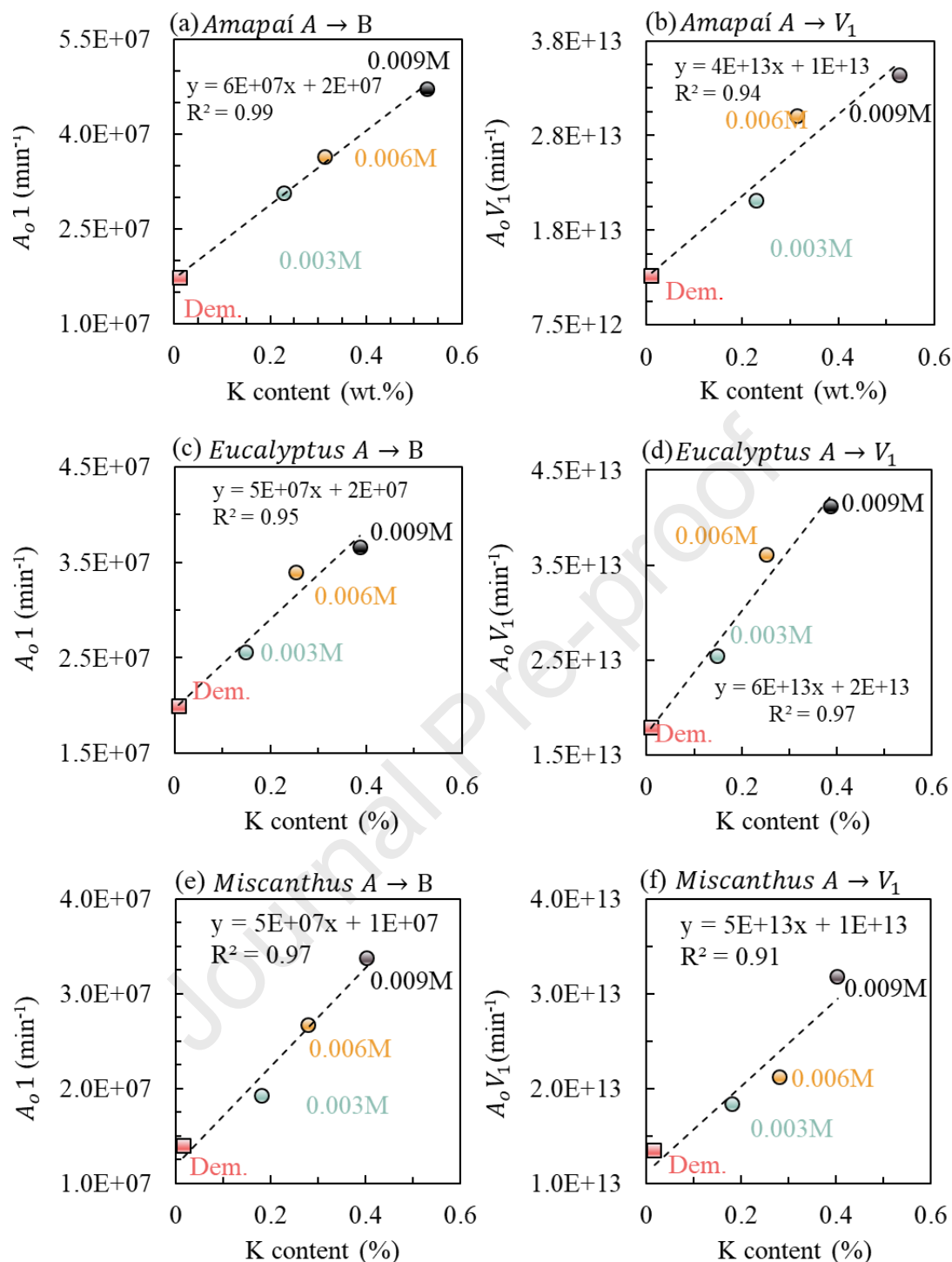
962

Journal Pre-proof



963

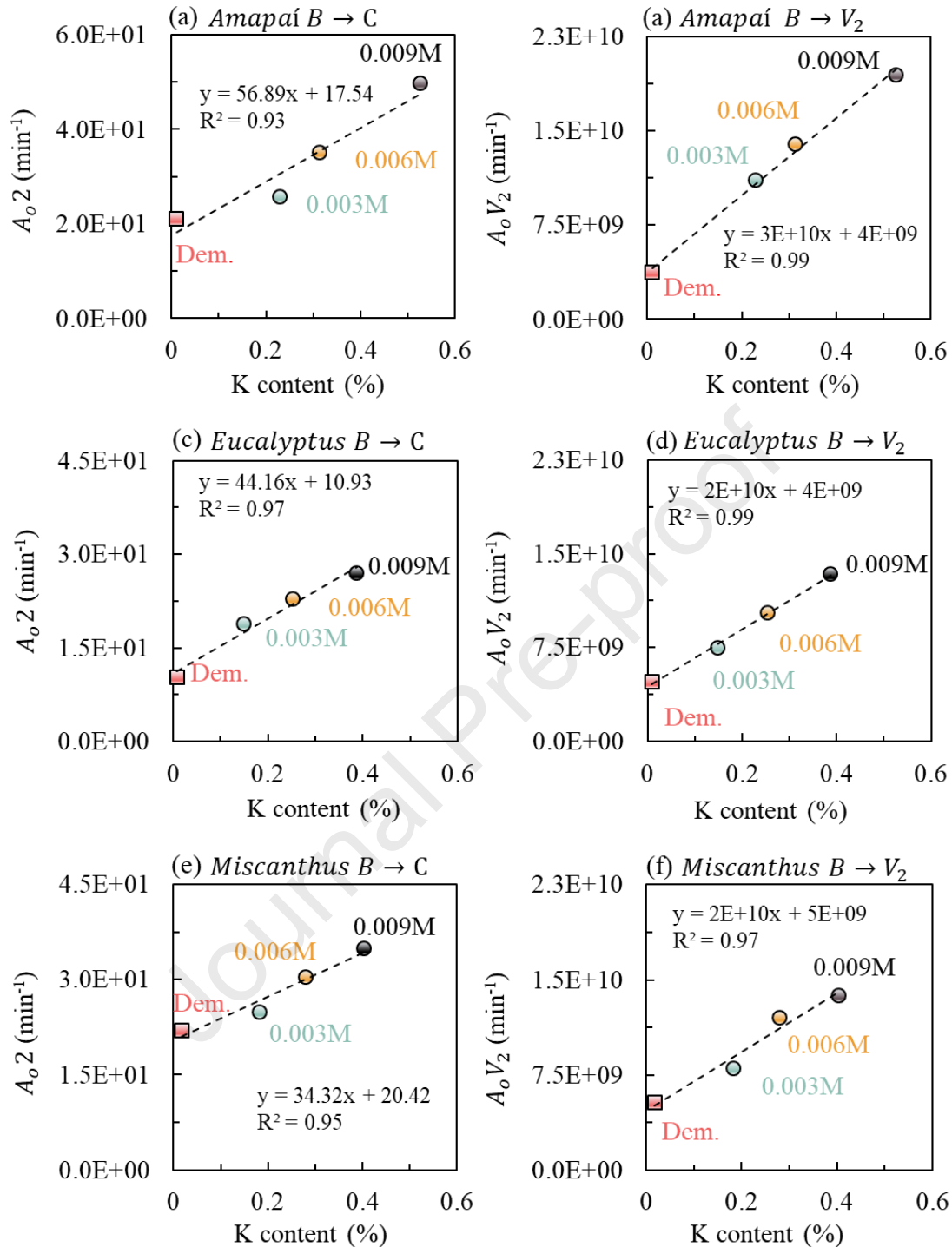
964 **Figure 02.** Experimental and numerically predicted solid yields determined with PRNP
 965 for demineralized and potassium impregnated *Amapaí* (a), *Eucalyptus* (b), and
 966 *Miscanthus* (c). Competition rates considering $K\%$ for *Amapaí* (d), *Eucalyptus* (e), and
 967 *Miscanthus* (f). To be noted that here, $t = 0$ corresponds to the treatment time at which
 968 the temperature is 170 °C. (2-column fitting)



969

970 **Figure 03.** Pre-exponential factors of demineralized and potassium impregnated samples
 971 (0.003, 0.006, 0.009M) as a function of potassium content (K%) for first step reactions
 972 $A \rightarrow B$ and $A \rightarrow V_1$ for *Amapaí* (a)(b), *Eucalyptus* (c)(d), and *Miscanthus* (e)(f). (2-
 973 column fitting)

974

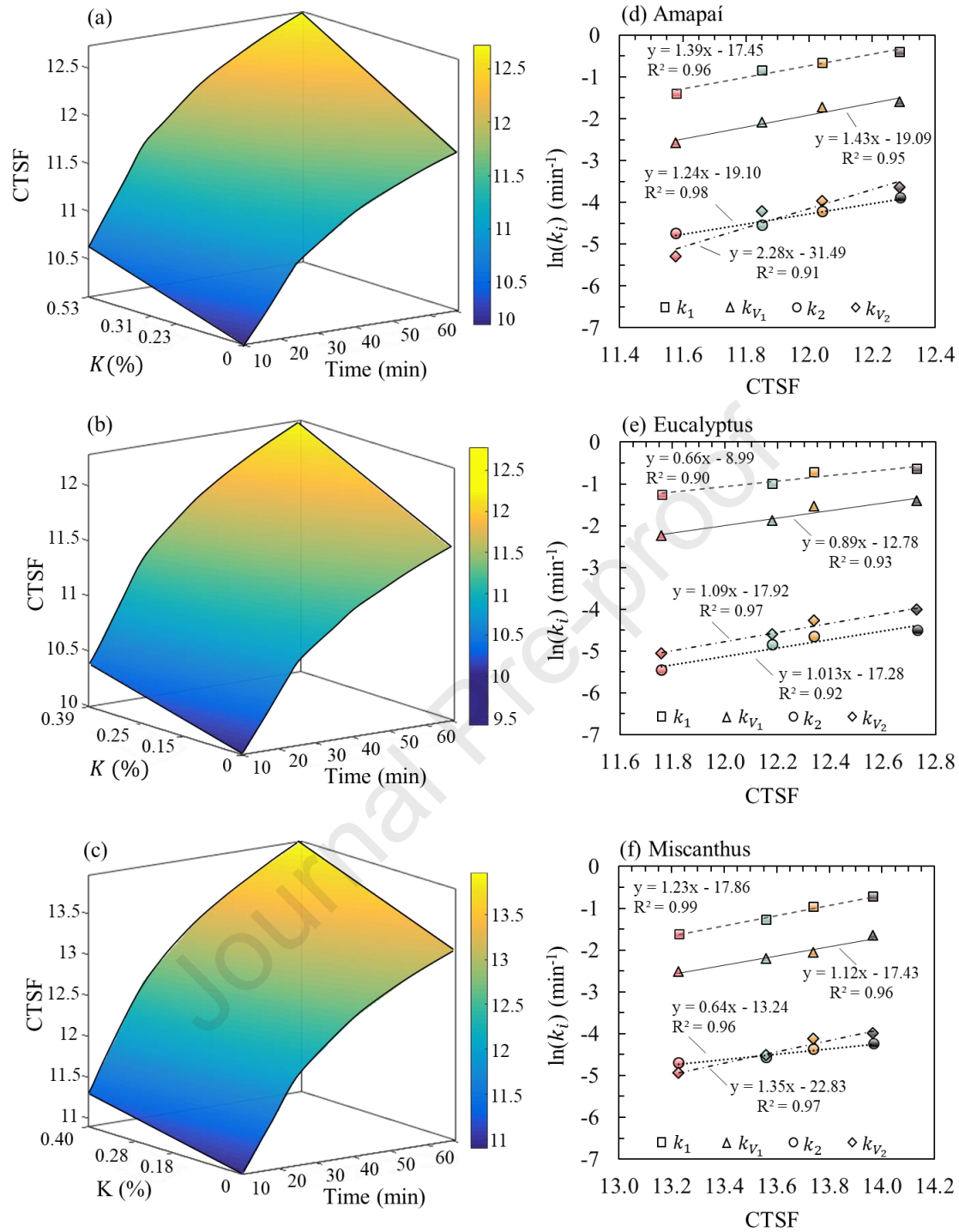


975

976 **Figure 04.** Pre-exponential factor constants of demineralized and potassium impregnated
 977 samples (0.003, 0.006, 0.009M) as a function of potassium content ($K\%$) for second step
 978 reactions $B \rightarrow C$ and $B \rightarrow V_2$, for *Amapáí* (a,b), *Eucalyptus* (c, d), and *Miscanthus* (e, f).
 979 (2-column fitting)

980

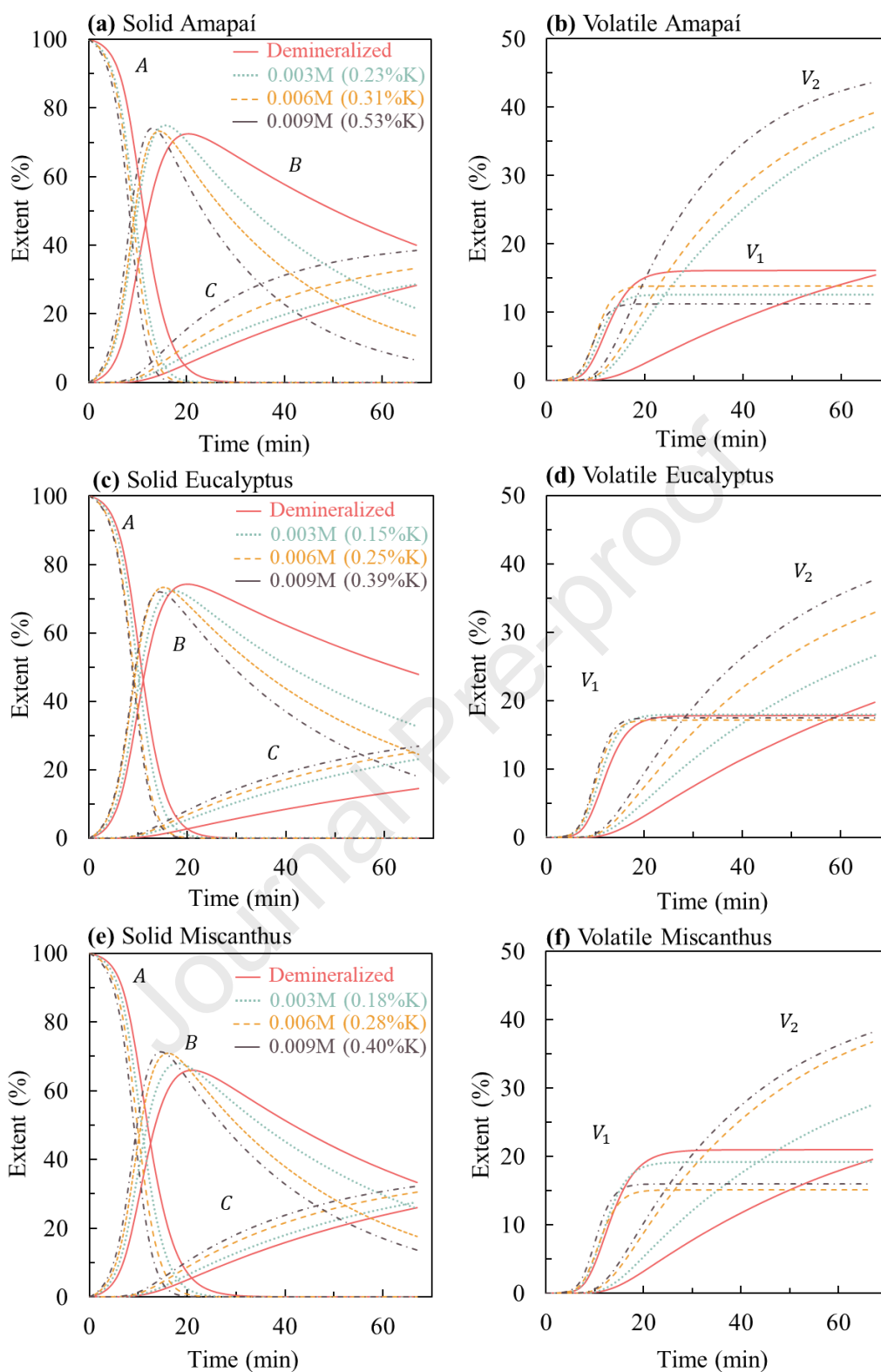
981



982

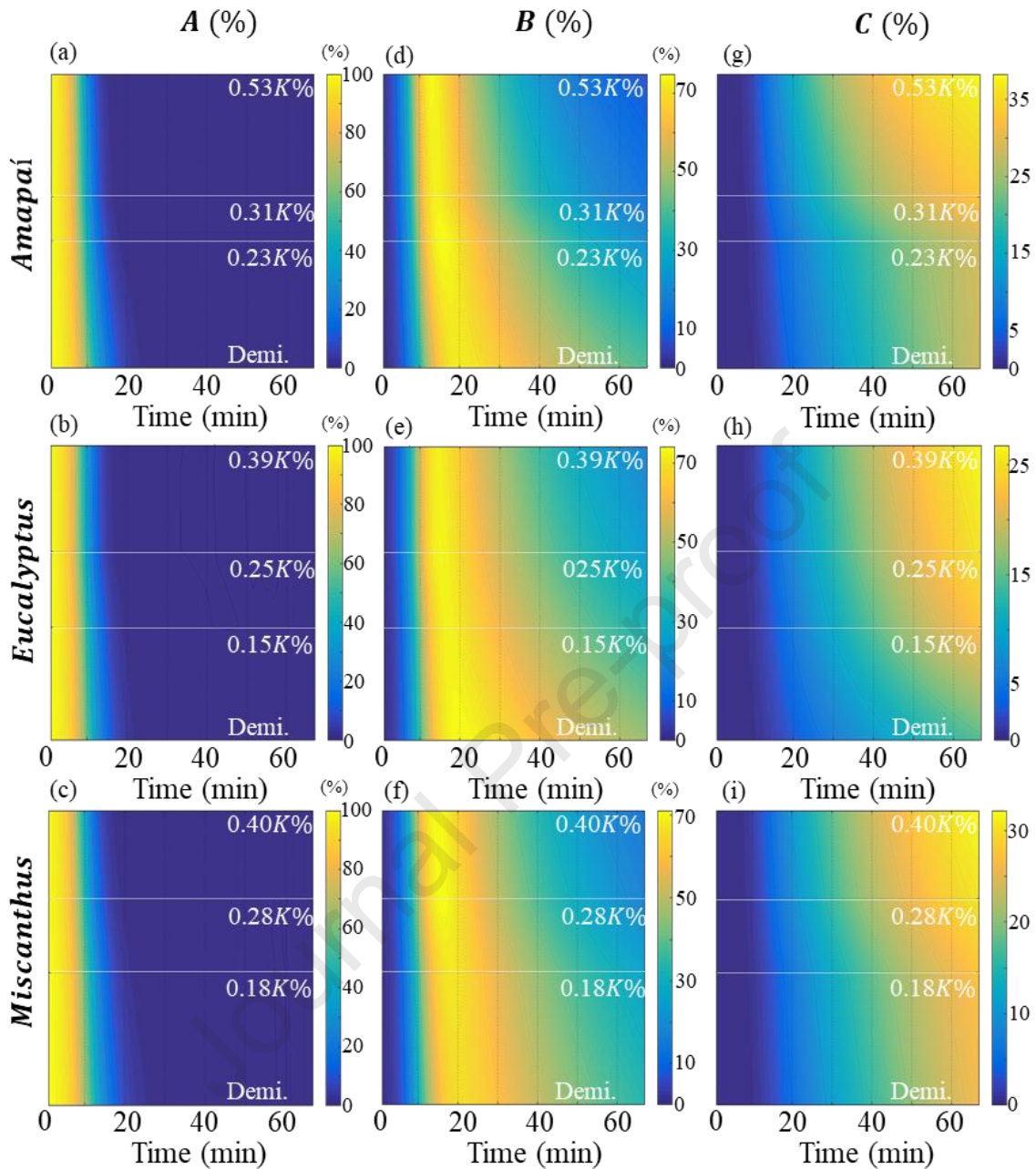
983 **Figure 05.** Numerically predicted CTSF for demineralized and potassium impregnated
 984 *Amapai* (a), *Eucalyptus* (b), and *Miscanthus* (c). Competition rates considering CTSF for
 985 *Amapai* (d), *Eucalyptus* (e), and *Miscanthus* (f). To be noted that here, $t = 0$ corresponds
 986 to the treatment time at which the temperature is 170 °C. (2-column fitting)

987



988

989 **Figure 06.** Solid and volatile pseudo-component evolution for demineralized and
 990 potassium impregnated samples of *Amapai* (a, b), *Eucalyptus* (c, d), and *Miscanthus* (e,
 991 f). To be noted that here, $t = 0$ corresponds to the treatment time at which the temperature
 992 is 170 °C. (2-column fitting)

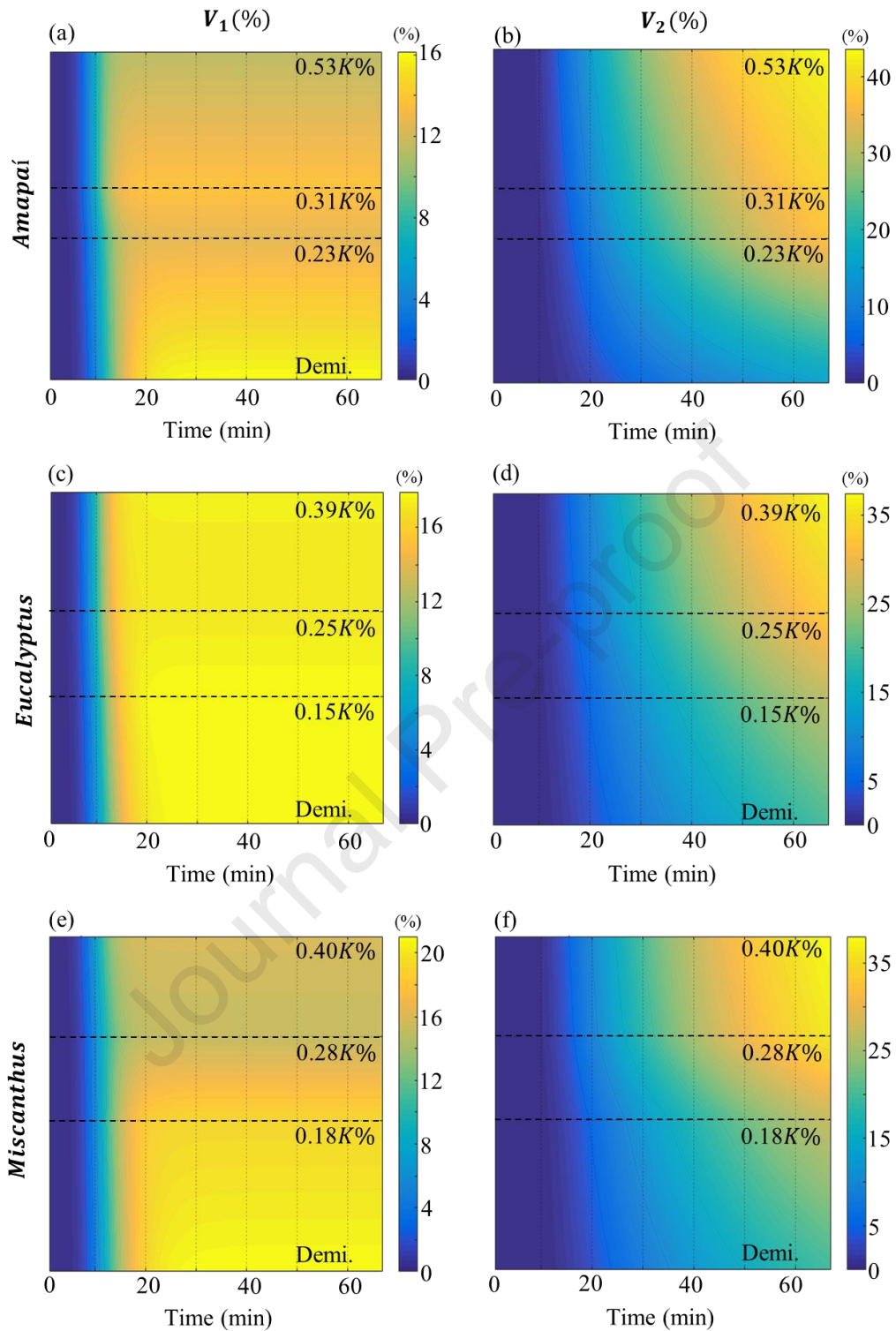


993

994 **Figure 07.** Solid pseudo-component (*A*, *B* and *C*) contour mapping according to the
 995 biomass species and potassium concentrations. To be noted that here, $t = 0$ corresponds
 996 to the treatment time at which the temperature is 170 °C. (2-column fitting)

997

998

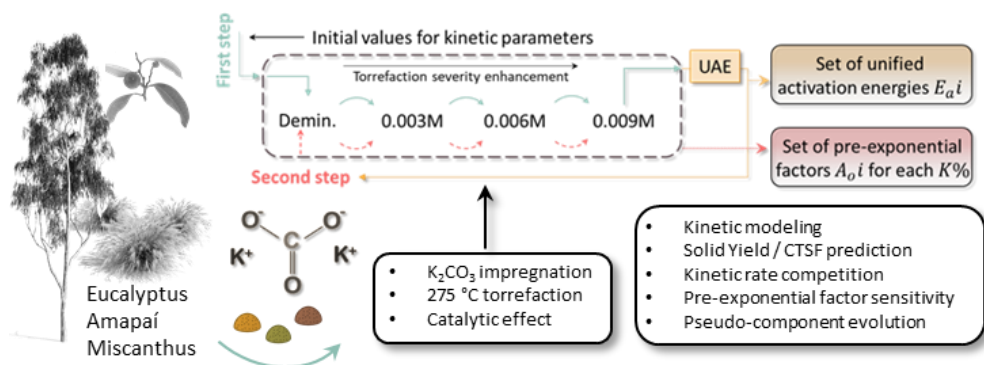


999

1000 **Figure 08.** Volatile pseudo-component (V_1 and V_2) contour mapping according to the
 1001 biomass species and potassium concentrations. To be noted that here, $t = 0$ corresponds
 1002 to the treatment time at which the temperature is 170 °C. (2-column fitting)

1003

Graphic abstract



1004

1005 **Highlights**

- 1006 • K_2CO_3 content in biomass influences its torrefaction kinetics;
- 1007 • A potassium responsive numerical path is proposed to model the torrefaction
- 1008 kinetics;
- 1009 • Pre-exponential factors increased linear correlation with $K\%$;
- 1010 • A significant linear correlation is observed for reaction rates with CTSF;
- 1011 • The catalytic impact on the pseudo-component evolution was assessed.

1012

1013 **Credit Author Statement (Author - Contribution)**

1014 **Edgar A. Silveira:** Conceptualization, Investigation, Formal analysis, Methodology,
1015 Writing - original draft.

1016 **Lucélia A. Macedo:** Data curation, Investigation, Methodology, Formal analysis,
1017 Writing - review & editing.

1018 **Patrick Rousset:** Writing - review & editing, Project administration, Supervision.

1019 **Kevin Candelier:** Validation, Writing - review & editing.

1020 **Jean-Michel Commandré:** Writing - review & editing, Project administration.

1021 **Luiz Gustavo O. Galvão:** Writing - review & editing.

1022 **Bruno S. Chaves:** Writing - review & editing.

1023

Highlights

- K_2CO_3 content in biomass influences its torrefaction kinetics;
- A potassium responsive numerical path is proposed to model the torrefaction kinetics;
- Pre-exponential factors increased linear correlation with $K\%$;
- A significant linear correlation is observed for reaction rates with CTSF;
- The catalytic impact on the pseudo-component evolution was assessed.

Declaration of interests

The authors declare that they have no known competing financial interests or personal relationships that could have appeared to influence the work reported in this paper.

The authors declare the following financial interests/personal relationships which may be considered as potential competing interests:

Journal Pre-proof